Anal. Methods Environ. Chem. J. 8 (2) (2025) 106-130

AMECJ

Research Article, Issue 2
Analytical Methods in Environmental Chemistry Journal
Journal home page: www.amecj.com/ir

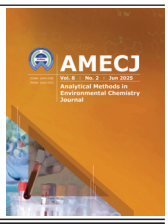

# Removal of heavy metal ions using surface-modified melamine magnetite nanoparticles as effective adsorbents prior to determination by atomic absorption spectroscopy

**Nada Qasim Jebur [a], Ali Abdulrazzaq Abdulwahid [a,**], and Hanna S. Abbo [a]**
[a] *University of Basrah, College of Science, Chemistry Department - Basrah, Iraq*

**ARTICLE INFO:**
Received 15 Feb 2025
Revised form 20 Apr 2025
Accepted 23 May 2025
Available online 29 Jun 2025
---
**Keywords:**
Melamine magnetic nanocomposites,
Heavy metal,
Flame atomic absorption spectroscopy,
Isotherm,
Thermodynamic

**ABSTRACT**
The melamine magnetic nanocomposite adsorbents were synthesized using the hydrothermal method with melamine, ethylene diamine tetraacetic acid, and 3,3'-diaminobenzidine. The adsorption efficiencies for the removal of cadmium and lead ions from aqueous solutions were investigated. The adsorbents were characterized using FTIR, high-resolution transmission electron microscopy (HRTEM), and energy-dispersive X-ray (EDX). Batch systems were carried out, and different operation parameters were optimized, including pH, agitation time, and temperature. The concentrations of heavy metal ions were determined with flame atomic absorption spectroscopy (F-AAS). It was observed that maximum removal efficiency was achieved at pH 8.0 and 5.0, with agitation times of 6, 3, and 1 hours for $Cd2^{+}$ and 2, 1.5, and 1 hours for $Pb2^{+}$ respectively. Langmuir, Freundlich, Dubinin–Radushkevich, and Temkin isotherm models were applied, and the results showed that Langmuir was fitted very well for all adsorption systems. According to the linearized Langmuir equation, $q_{max}$ cadmium and lead ions were 49.26, 76.92and 256.4 mg $g^{-1}$ and 188.7, 294.1, and 588.2 mg $g^{-1}$ for M@F, M@EDTA@F, and M@EDTA@Am@F, respectively. The kinetic models were conducted to understand the adsorption mechanisms, pseudo-second-order model agreed well with experimental data for cadmium and lead ions overall adsorbents. Adsorption systems results were evaluated by calculating thermodynamic parameters, including enthalpy, entropy, changes in free energy, and activation energy (Ea).

## 1. Introduction

Many organic and inorganic contaminants are harmful to the environment. Heavy metal ions pose the greatest threat to the modern world because of their high toxicity and carcinogenic potential. Heavy metal contamination is caused by human activity's impact on the ecosystem's food chain. Several different industries emit heavy metals into the environment, including the chemical, textile, tannery, plastic, mining, battery, paint, and pulp industries [1]. The release of harmful metals into streams may impact the quality of the water supply. Lead, arsenic, mercury, chromium, and cadmium are a few of the dangerous heavy metal ions that could endanger human health. Heavy metal ions build up in living things and are not recyclable [2]. The use of heavy metal ions has been steadily increasing as a result of increased industrial activity,

*Corresponding Author: Ali Abdulrazzaq Abdulwahid
Email: ali.abdulwahid@uobasrah.edu.iq
https://doi.org/10.24200/amecj.v8.i02.1066

which is causing pollution of water streams on a daily basis. Due to their inability to biodegrade, the heavy metal ions are potent toxicants. Heavy metal ions are also known to cause cancer. Heavy metal ions in water systems are alarmingly greater than what is allowed and can lead to various ailments [3]. Among the heavy metals, it has been demonstrated that lead (Pb) and cadmium (Cd) are incredibly harmful to people. Because of its impact on human health and the environment, cadmium is one of the most hazardous metals. Teratogenic, nephrotoxic, hepatotoxic, and carcinogenic consequences result from its accumulation in many tissues and organs. When individuals are exposed to cadmium, they may experience harmful effects such growth retardation and liver and kidney poisoning. Cd damages DNA, interferes with DNA repair processes, and produces reactive oxygen species at the molecular level, all of which can lead to cancer [4]. The second most hazardous element, lead, is toxic to ecosystems and exhibits persistent distribution traits. Because of this metal's ability to pass from crops to humans and bioaccumulate, more and more research has been conducted on its relationship to food safety [4]. The primary anthropogenic sources of lead include industrial and municipal discharges, as well as agricultural inputs [5]. Pb's negative consequences on human health include kidney failure, hypertension, and harm to the neurological and digestive systems. Cancer, reticulocytosis, and hematopoietic problems; in children, it can also result in attention deficit, hearing loss, and delayed mental development [6]. Additionally, Pb causes oxidative stress and makes people more susceptible to it, which raises estrogen levels and is a significant risk factor for breast cancer [7]. Furthermore, high blood levels of lead have an impact on postnatal development, behavior, and cognitive function; they can delay puberty and impair newborns' and children's hearing [8]. Moreover, the negative consequences of Pb pollution include anorexia, anemia, brain damage, vomiting, and disorders of the neurological and circulatory systems [9]. Heavy metal ions and other pollutants can be removed using various techniques, such as extraction, solid phase extraction, UV semi-degradation, adsorption, and UV photo-catalytic degradation-adsorption [10-19]. However, these techniques are rarely employed because of their limited viability and high cost. Due to low cost and excellent efficiency, adsorption techniques are one of the preferred ways to remove heavy metals. The quest for efficient adsorbents is still ongoing. However, adsorption techniques are the most popular and affordable alternative technology.

## 2. Experimental

### *2.1. Materials and Instruments*

Melamine was purchased from Merck (Germany). The Concentrated sulfuric acid ($H_2SO_4$, CAS Number: 7664-93-9), hydrochloric acid (HCl, 36%, CAS Number: 7647-01-0), sodium hydroxide (NaOH, CAS Number: 1310-73-2), sodium carbonate, N, N′-dicyclohexylcarbodiimide (DCC, CAS Number: 538-75-0), $(NH_4)_2Fe(SO_4)_2.6H_2O$, and $FeCl_3$ were purchased from BDH. Ethylenediaminetetraacetic acid (EDTA, CAS Number: 6381-92-6, 99.0%) was also obtained from Sigma-Aldrich. 3,3`-diaminobenzidine was prepared from Sigma Aldrich, and the other materials were purchased from various commercial companies. All other reagents used in this study were analytical grade, and distilled or double-distilled water was used to prepare all solutions. A standard solution of cadmium and lead, 1000 mg $L^{-1}$ was made for the adsorption experiments, and the required concentrations were provided by diluting it with distilled water.

Fourier-transform infrared spectroscopy (FTIR) of the prepared adsorbents was recorded by an FTIR-8101M Shimadzu spectrometer (Japan) with a KBr pellet in the region (400–4000 $cm^{-1}$) to investigate the chemical structures. The German (ALPHA II) device from the BRUKER company was also used to measure the prepared compounds. The adsorbent's structure and morphology were identified using a FEI NOVA NanoSEM 450 (Netherlands), and field emission scanning electron microscopy (FESEM) under vacuum at an operating voltage of 10 kV. Patterns of X-ray diffraction

(XRD) of the materials were recorded by a Rigaku X-ray powder diffraction diffractometer (Japan) using Cu Kα radiation with a wavelength of 1.54 Å at a scanning speed of 2 $min^{-1}$ from 5° to 80°. Flame Atomic Absorption Spectroscopy (F-AAS, Phoenix-986 Spectrophotometer) prepared by Biotech Engineering Management Co., Ltd. The specimen was measured using Transmission Electron Microscopy (TEM, AB912LEO).

### *2.2. Synthesis of M@F*

The melamine@ $Fe_3O_4$ composite (M@F) was synthesized following the hydrothermal method. Melamine (0.1 g) was sonicated in ethylene glycol (70 mL). Subsequently, $FeCl_3$(2.0mol), $(NH_4)_2Fe(SO_4)_2.6H_2O$ (1.0 mol), ammonium hydroxide (15 mL, 30%V/V), and sodium acetate (16 mol) were added to the solution of melamine, which was then loaded into (100 mL) Teflon vessels sealed and placed in oven with temperature (200$^0$C) for six hours. The mixture was cooled down to room temperature. Then, after the mixture was separated magnetically, it was washed with distilled water several times to remove the remaining ethylene glycol. The preparation route can be shown in Scheme 1.

### *2.3. Synthesis of Melamine Formaldehyde*

Melamine (6.3g, 0.05 mol) and formaldehyde (9.0g, 0.3 mol) were mixed in 50 mL of distilled water, which was adjusted to pH 8.0-9.0 using a 10% sodium carbonate solution. The melamine-formaldehyde (MFO) prepolymer was prepared under alkaline conditions. After stirring for 1.5 hours at 80.0 and 90.0°C, the MFO was obtained. Scheme 1 illustrates the preparation route.

### *2.3.1.Synthesis of M@EDTA@F*

For the synthesis of melamine formaldehyde @ EDTA@F composite, sulfuric acid (Conc.; 10 mL) was added to a stirred suspension of M-FO (0.306g, 1.0 mol) and EDTA (2.232g, 6.0 mol) in 50.0 mL distilled water. The suspension was stirred and heated at 60°C for 10 hours. Next, the solution was filtered. The filtrate was concentrated under vacuum for 6 hours to yield M@EDTA, illustrated in Scheme 1. M@EDTA@F was prepared by the hydrothermal method.

### *2.4. Synthesis of M@EDTA@Am@F*

For the synthesis of melamine formaldehyde@ EDTA@3,3`-diaminobenzidine@$Fe_3O_4$ composite, 1.854g, 1.0 mol of (M@EDTA) was dissolved by ultrasonication in 50 mL of distilled water in 3 hours. To activate the carboxyl groups of the (M@EDTA), a solution of (0.206g, 1.0 mol) N,N´-dicyclohexylcarbodiimide (DCC) was mixed with the (M@EDTA) dispersion, and the mixture was rapidly agitated for 2 hours. A 2% NaOH solution was used to bring the pH down to 7.0. After that, the activated (M@EDTA) solution with (3.852g, 18.0 mol) of 3,3'-diaminobenzidine (Am) was mixed for 20 minutes using an ultrasonicator. Subsequently, the amalgamated solutions were stirred for 3 hours at 60 $^0$C. After filtering, the precipitate was washed twice: once with distilled water and once with a solution of 10% NaOH until the pH was about 7.0. Following production, M@EDTA@Am. was dried in a vacuum oven. Scheme 1 shows the path of preparation. M@EDTA@AM.@F. @ F was prepared by the hydrothermal method.

### *2.5. Adsorption experiments*

Batch adsorption experiments [20-22] of cadmium and lead ions were conducted to assess the adsorption characteristics and adsorption-influencing variables, the removing efficiency of synthesized adsorbents were examined by shaking 0.05 g of each adsorbents with 50 mL of ions solutions at initial concentrations, 50.0, 100.0, and 200.0 $mg.L^{-1}$ of cadmium ion and 100.0, 250.0, 400.0 $mgL^{-1}$ of lead ion were an initial concentrations for M@F, M@EDTA@F, M@EDTA@Am.@F adsorbents respectively. The adsorption experiments were carried out on a thermostat shaker set to 27°C and 200 rpm for a predetermined time. When agitation time was complete, the adsorbents were separated magnetically from the solution, and the concentrations of remaining ions were determined with flame atomic absorption spectroscopy. The

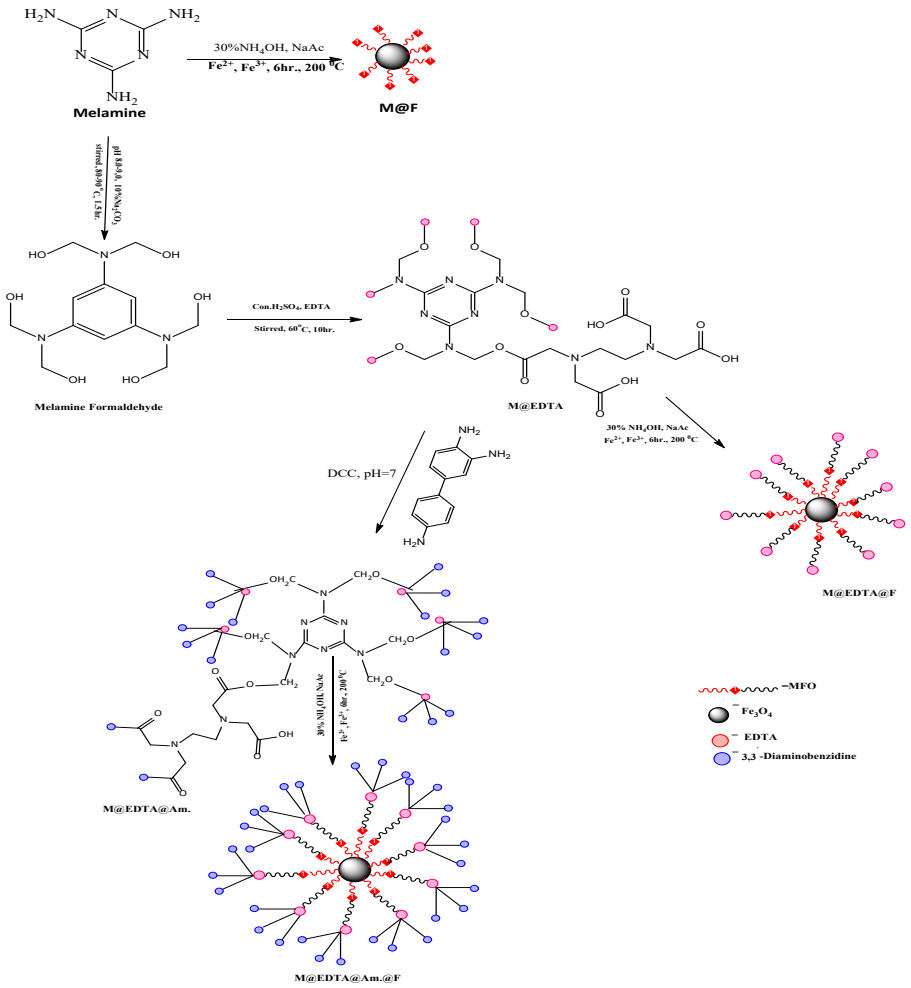


**Scheme 1**. Synthetic routes for preparing M@F, M@EDTA@F, and M@EDTA@Am.@F

amount of the ion on the adsorbents was evaluated using Equation 1. The adsorption isotherm studies were applied at optimum conditions, including an agitation time of 6, 3, and 1 hour at pH 8.0 for cadmium ion and of 2, 1.5, and 1 hour at pH 5.0 for lead ion, onto M@F, M@EDTA@F, and M@EDTA@Am@F, respectively. The varying initial concentrations of cadmium ion (50.0-200.0 mg $L^{-1}$) and lead ion (100-400 mg $L^{-1}$) were used at constant temperature (27◦C). To study adsorption kinetics and to calculate enthalpy (ΔH°), entropy (ΔS°), and free energy (ΔG°), the experiments were conducted at 27°C, 40°C, and 55°C, with 0.05 g of adsorbents.

$$q = \frac{(C_o - C_e)}{m} V \qquad \text{(Eq.1)}$$

Where $C_0$ and $C_e$ (mg $L^{-1}$) are the initial and equilibrium concentrations of cadmium and lead ions in the solution, V (in L) is the volume of metal ions solutions, m (in g) is the mass of the used adsorbents, and (in mg of ions per g of adsorbent) is the amount of adsorbed metal ions per gram of adsorbent (adsorption capacity).

## 3. Results and Discussion

### *3.1. FTIR characterization*

The FTIR spectra showed the characteristic bands of the M@F (Fig. 1a). An absorption band around 850 $cm^{-1}$ is assigned to the out-of-plane bending vibration of the triazine ring. The adsorption bands at 1064 $cm^{-1}$ and 1624 $cm^{-1}$ are assigned to stretching and bending vibrations for the C-N bond of the N-C–N of the triazine ring, respectively. The peaks at 3384 and 3488 $cm^{-1}$ are associated with symmetrical

and asymmetrical stretching vibrations of primary amines. The peak at 578 $cm^{-1}$ refers to iron oxide [23]. The melamine formaldehyde (MFO) spectrum peaks at 3348 $cm^{-1}$ (Fig. 1 b), which is assigned to the stretching vibration of O-H bonds. In contrast, the absorption peaks at 2900 and 1346 $cm^{-1}$ can be assigned to the stretching and bending vibration of C-H in the alkane, respectively. The peaks at 1562 and 1490 $cm^{-1}$ are attributed to the stretching vibration of C=N and C-N of the heterocyclic, respectively. [24]. FTIR spectrum of M@EDTA shown in 1.c. displays a band at 1631 $cm^{-1}$correspond to C=O ester group, a peak at 1376 $cm^{-1}$ assigned to $CH_2$ stretching vibration. The peak at 3586 $cm^{-1}$ refers to the OH carboxylic acid stretching vibration, and a peak at 1083 $cm^{-1}$ refers to the C-O stretching vibration [25]. The IR spectrum of M@EDTA@Am. Figure 1d shows a combination of M@EDTA and Am(amine) characteristic peaks. The absorbance bands at 3360-3286, 1622, and 1572 $cm^{-1}$ correspond to the N–H stretching vibration, C=O stretching of –NHCO–, and N–H bends of $–NH_2$ respectively [26]. The O–H peak shift from around 3403-3586 $cm^{-1}$ to (3360-3286) $cm^{-1}$ confirms the interaction between M@ EDTA and Am(A). All as-synthesized magnetic nanocomposites display the characteristic absorption of Fe-O stretching vibrations at 539 $cm^{-1}$ and 546 $cm^{-1}$ (Fig. 1e and 1f).

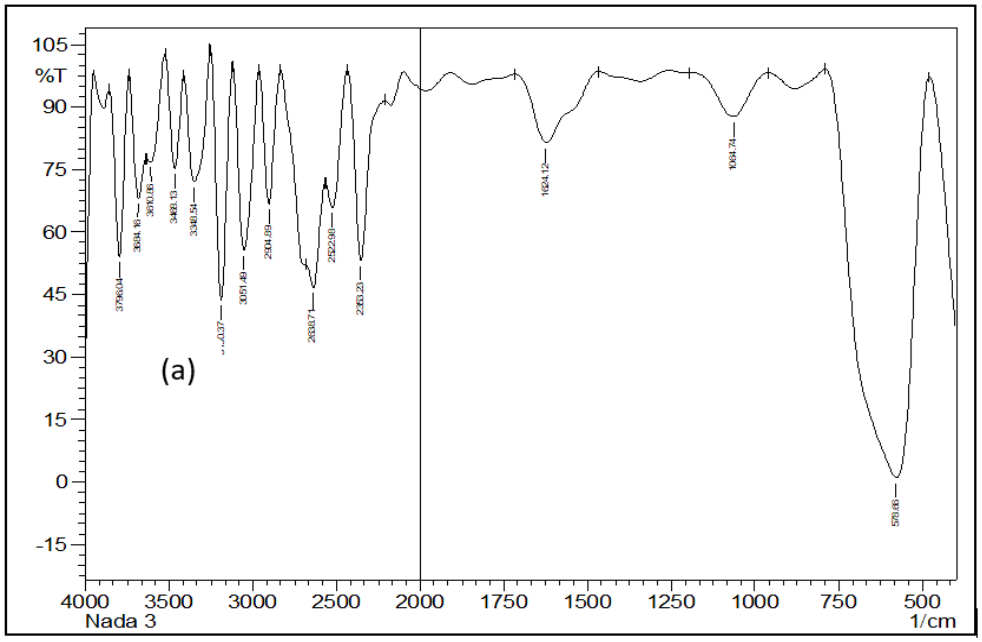


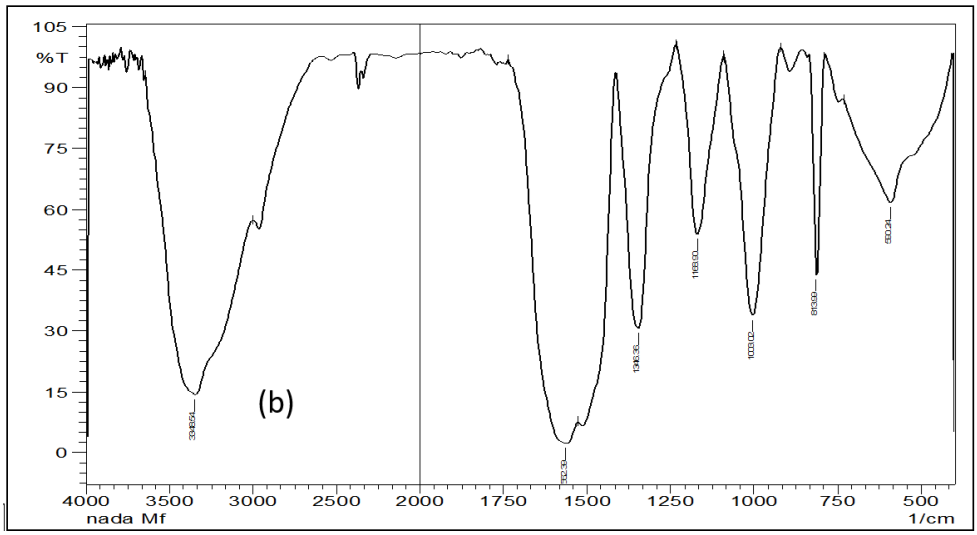

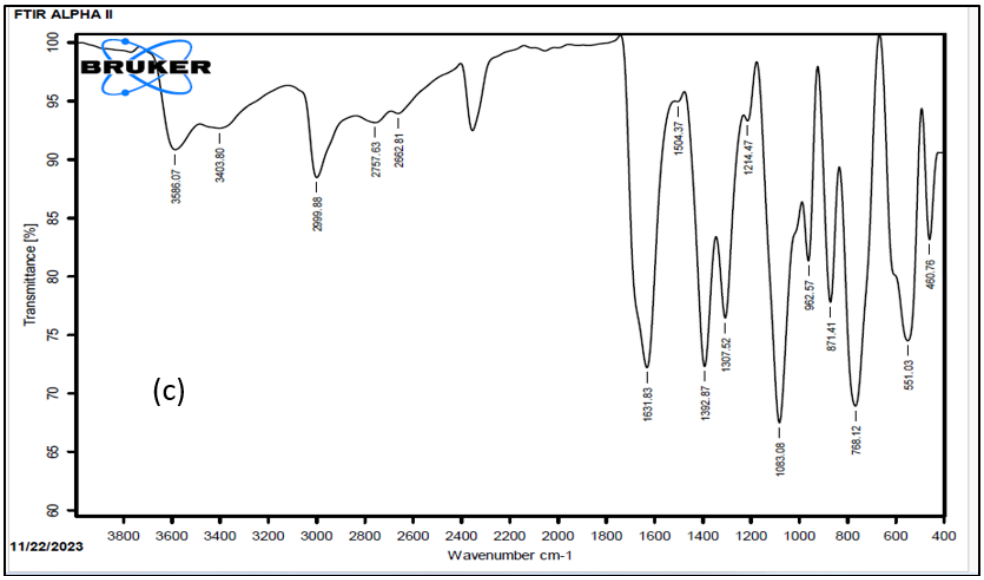
FTIR ALPHA II
BRUKER
Transmittance [%]
3586.07
3403.80
2999.88
2757.63
2662.81
1631.83
1504.37
1392.87
1307.52
1214.47
1063.08
962.57
871.41
768.12
551.03
460.76
(c)
11/22/2023
Wavenumber cm-1

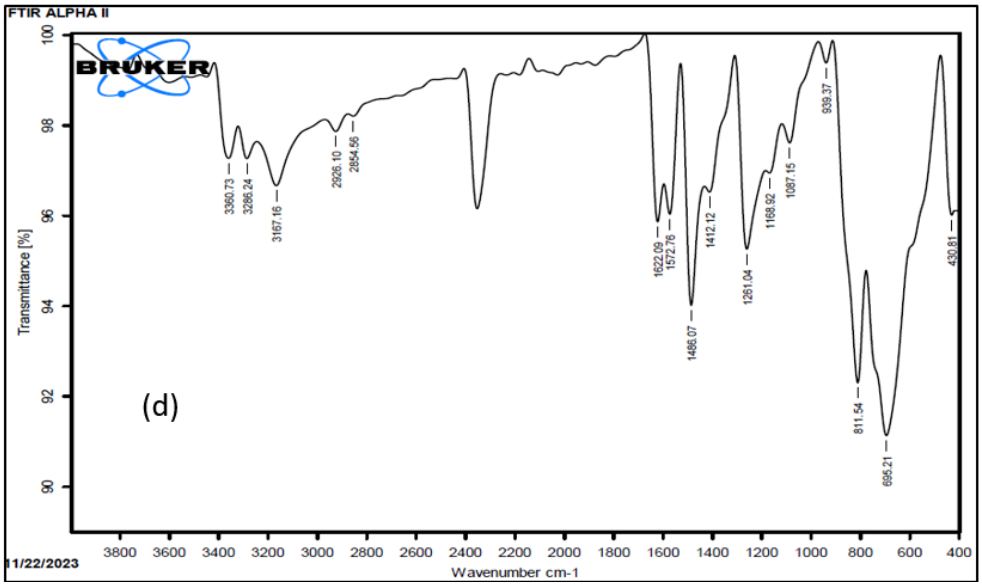
FTIR ALPHA II
BRUKER
Transmittance [%]
3360.73
3286.24
3167.16
2926.10
2854.56
1622.09
1572.76
1486.07
1412.12
1261.04
1168.92
1087.15
939.37
811.54
695.21
430.81
(d)
11/22/2023
Wavenumber cm-1

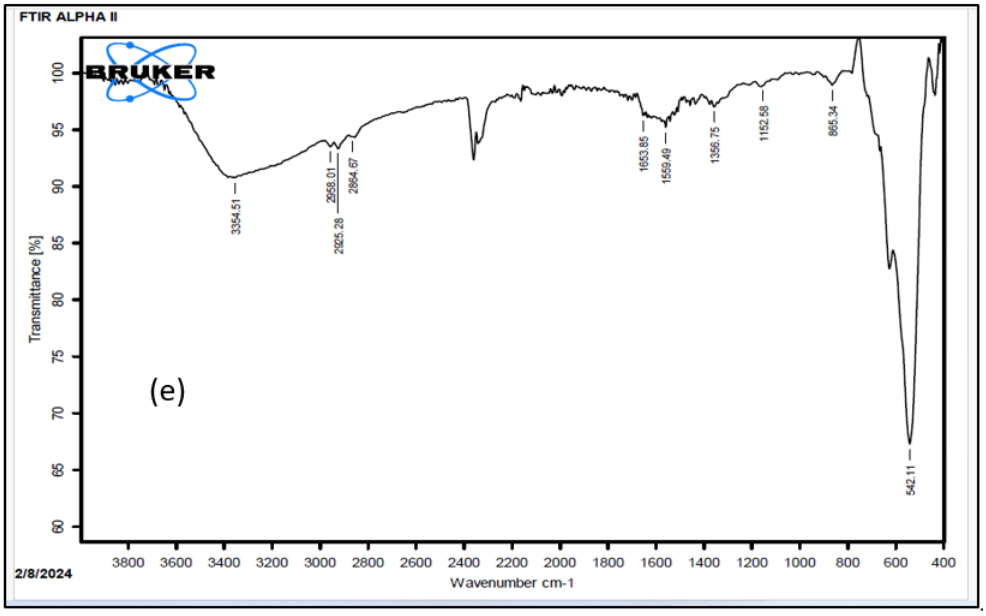
FTIR ALPHA II
BRUKER
Transmittance [%]
3354.51
2968.01
2925.28
2864.67
1653.85
1559.49
1356.75
1152.58
865.34
542.11
(e)
2/8/2024
Wavenumber cm-1

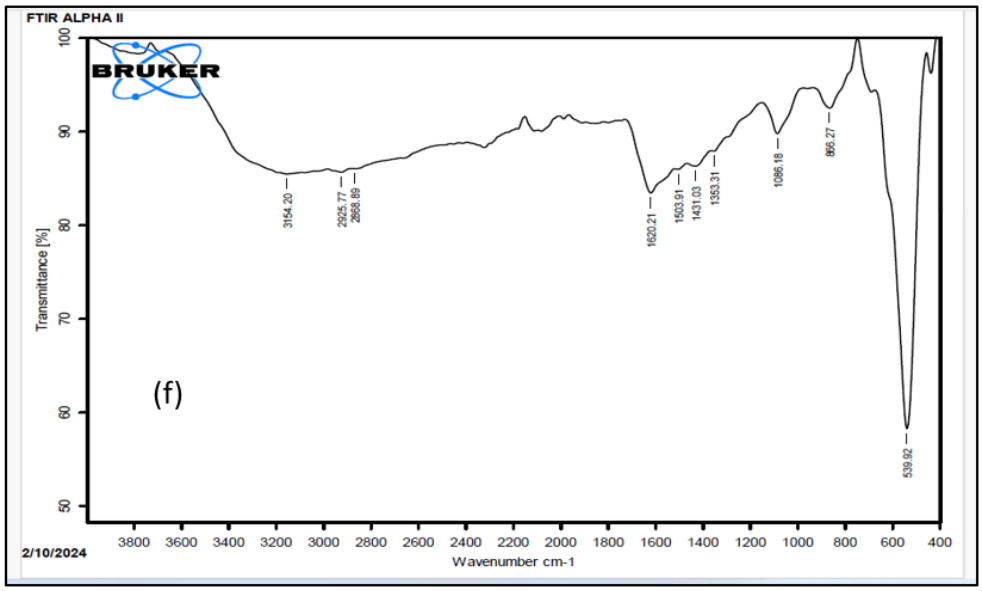


**Fig.1.** FTIR spectra of (a) M@F, (b) MFO (c) M@EDTA, (d) M@EDTA@Am(e) M@EDTA@F, and (f) M@EDTA@Am@F

### *3.2. High-Resolution Transmission Electron Microscopy (HRTEM)*

High Resolution Transmission Electron Microscopy (HRTEM) is the most common technique to analyze nanoparticle size and shape, since it provides direct images of the sample and the most accurate estimation of the nanoparticle homogeneity. The main advantage of this approach is its amazing capacity to penetrate the sample with an electron beam, allowing for a thorough examination of its internal structure. Figure 2 shows clear morphological changes of nanocomposites. Magnetite nanoparticles are widely distributed on the shell surface of the matrix. Furthermore, $Fe_3O_4$ NPs are well wrapped by the shell layer. The shell is adsorbed by electrostatic and hydrogen bonding to the surface of the magnetite. Transmission electron microscopy of the as-synthesized MNPs indicates that MNPs are of a spherical or multifaceted shape, with a median size of nm (N =18.4), calculated by the ImageJ program. The selective area electron diffraction (SAED) also indicated the crystalline structure of $Fe_3O_4$ nanoparticles depicted in Figure 2. The dark field revealed a single crystal structure of $Fe_3O_4$ nanoparticles. The image exhibits well-defined and distinct lattice fringes, which can be attributed to the Miller indices and corresponding interplanar spacings of the (1 1 1), (2 2 0), (3 1 1), (4 0 0), (5 1 1), and (4 4 0) planes. indicate that the NPs are highly poly-crystalline in nature, which is in good agreement with the XRD results.

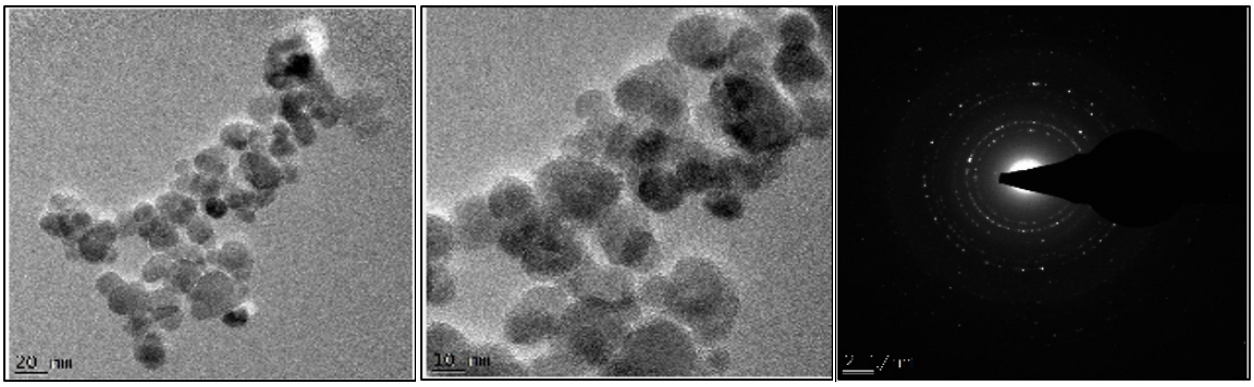


**Fig. 2**. HRTEM images of M@EDTA@Am.@F.

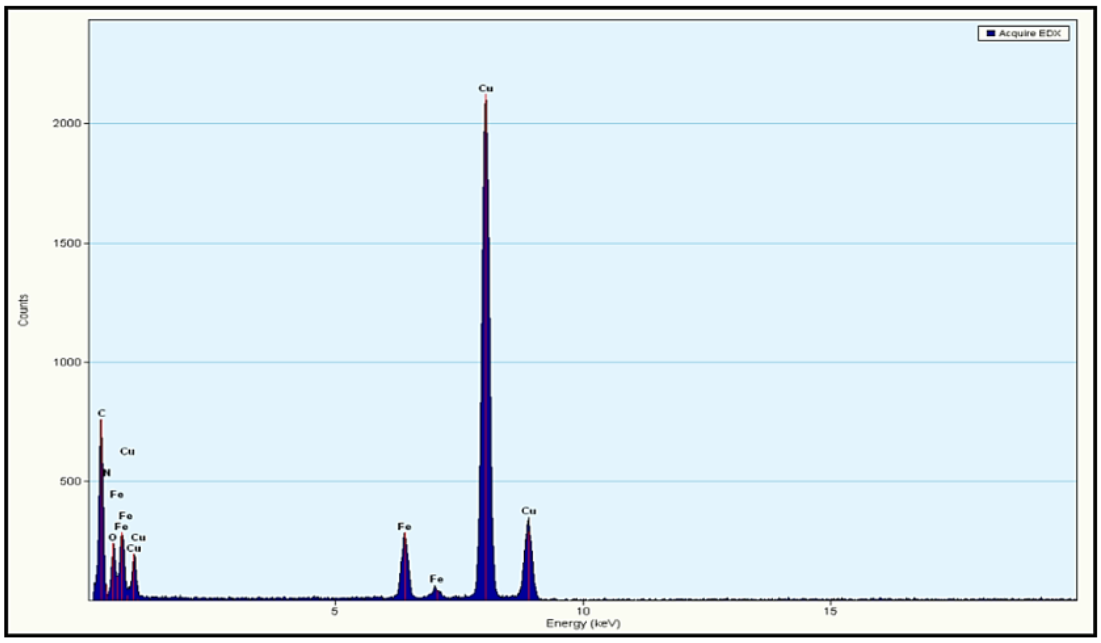


**Fig. 3**. EDX of M@EDTA@Am.@F

### *3.3. Energy Dispersive X-ray Spectroscopy*

The presence of elements in the structures of compounds was investigated using X-ray energy dispersive spectroscopy (EDX) analysis. The elemental analysis of the nano composite by EDS revealed the presence of Fe, O, H, C, and N as the only components of the particles, as shown in Figure 3.

### *3.4. X-ray Diffraction Spectroscopy (XRD)*

Technology for X-ray diffraction (XRD) is a crucial diagnostic tool for nanoparticles and nanocomposites. X-ray diffraction (XRD) is a quick and non-destructive analytical technique that frequently yields precise results for identifying samples [27]. As shown in Figure 4, XRD analysis confirms that the produced MNPs primarily consist of magnetite. The obtained patterns displayed a high level of agreement with the data from the magnetite reference database (JCPDS card No. 19-0629) [28]. Notably, the as-synthesized samples exhibit excellent crystallinity with well-defined magnetite peaks, showcasing the high quality of these particles. The peaks can be indexed at the values of 2θ = 30.2° (220); 35.4° (311); 43.4° (400); 53.9° (422); 56.9° (511); and 62.6° (440), respectively, for the MNP-$Fe_3O_4$. Including melamine also caused a broad peak in the melamine modification patterns at 2θ = 20.3°. The results suggest that the synthesized $Fe_3O_4$ particles have homogeneous morphological properties and a high degree of crystallinity. These diffraction patterns are consistent with the calculated X-ray diffraction patterns reported in the literature [28]. The studied materials' average crystallite size, D (nm), was calculated using the Debye–Scherrer Equation 2 [29].

$$D = \frac{K_s . \lambda}{\beta . cos\theta} \quad \text{(Eq.2)}$$

Where D was the size of the crystal, λ was the wavelength for X-ray diffraction in (nm) for CuKα1, which is equivalent to 1.54060 Å translated to 0.154nm, and Ks is the constant, usually written as 0.9, which is related to the crystal structure's shape. The Full Width Half Maximum (FWHM) of spherical crystals with cubic unit cells in radian angle units is represented by β. This can be derived from each graph after converting each compound's X-ray diffraction spectroscopy to a radian angle. As a result, the 2θ was divided by

two and then multiplied by 0.01745329 to become θ. Furthermore, β was determined using the relationship [30] that follows:
1 Degree = 0.01745329 radians
θ in radian angle = (2θ/2 * 0.01745329)
β = Value of FWHM x 0.01745329

### *3.5. Optimization of adsorption parameters*

The batch systems were employed in adsorption experiments of cadmium and lead ions aqueous solutions, and the adsorption efficiencies were evaluated with respect to optimum pH, contact time, temperature, and the initial concentration ($C_0$).

#### *3.5.1.Effect of pH*

The effect of pH on the adsorption capacities qe evaluated. As shown in Figure 5, all adsorbents were studied at different values ranging from 2.0 to 8.0 for cadmium and 2.0 to 5.0 for lead because they precipitated as metal hydroxide above these values. Figures 5A and 5B show that the adsorption capacities were increasing gradually with pH increasing, at a strong acidic media there were an abundance of $H^+$ ions which compete cadmium and lead ions towards adsorbents surface resulting in decreasing the adsorption capacity, but when the pH increased the loading of cadmium and lead ions be more favorable, on the other hand at the elevation of pH values of the solution lead to a decrease in the solubility of ions, and ultimately leads to achieving maximum efficiency and adsorption capacity [31].

#### *3.5.2.Effects of Agitation Time and Temperature on the Adsorption:*

One of the most crucial factors in the adsorption process is the effect of the contact time between the adsorbent and the adsorbate, since determining the equilibrium contact time is critical in predicting the viability and performance of an adsorbent for a process [32]. The effect of contact time on the adsorption of cadmium ions onto M@F, M@EDTA@F, and M@EDTA@Am@F was studied at different temperatures, 27, 40, and 55 °C. The Figures 6 (A, B, C) and Figures 7(A, B, C) show the adsorption efficiencies of cadmium and

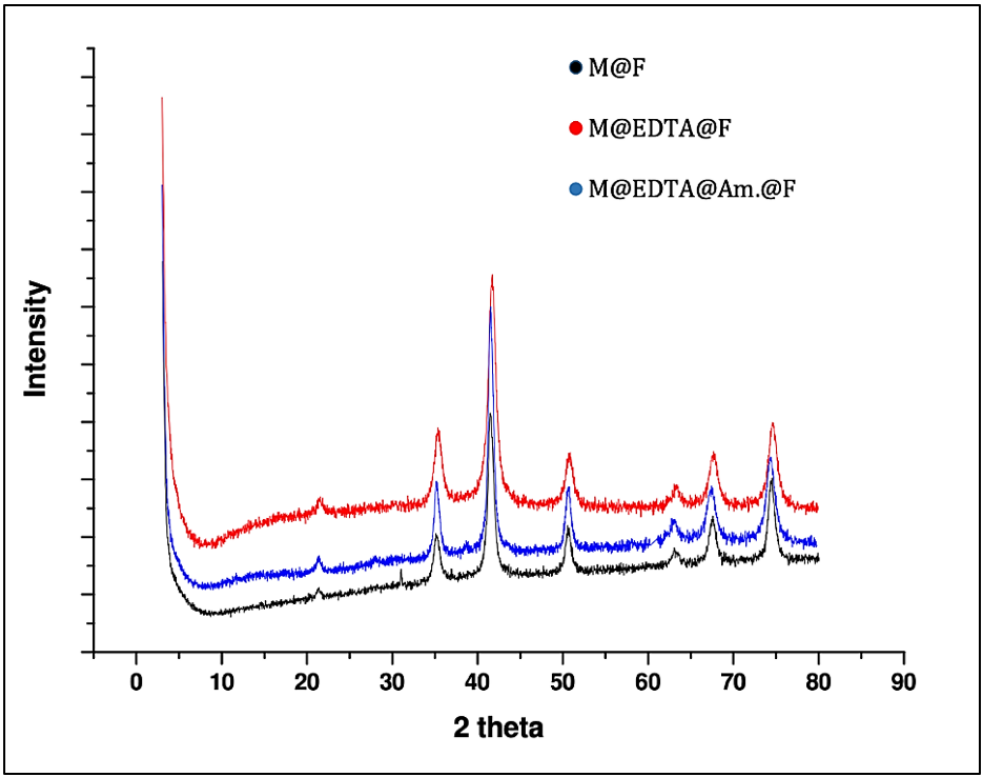


**Fig.4**. XRD of (a) M@EDTA, (b) M@EDTA@F (c) M@EDTA@Am.@F

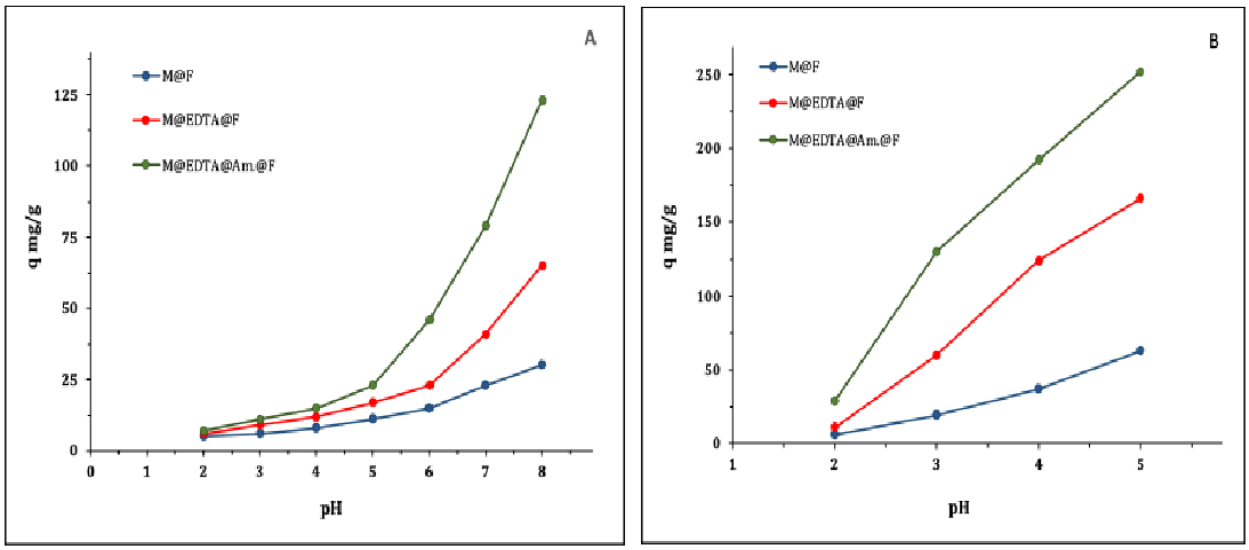


**Fig. 5**. Effect of pH for (A) Cadmium (B) Lead ion solution at 27°C

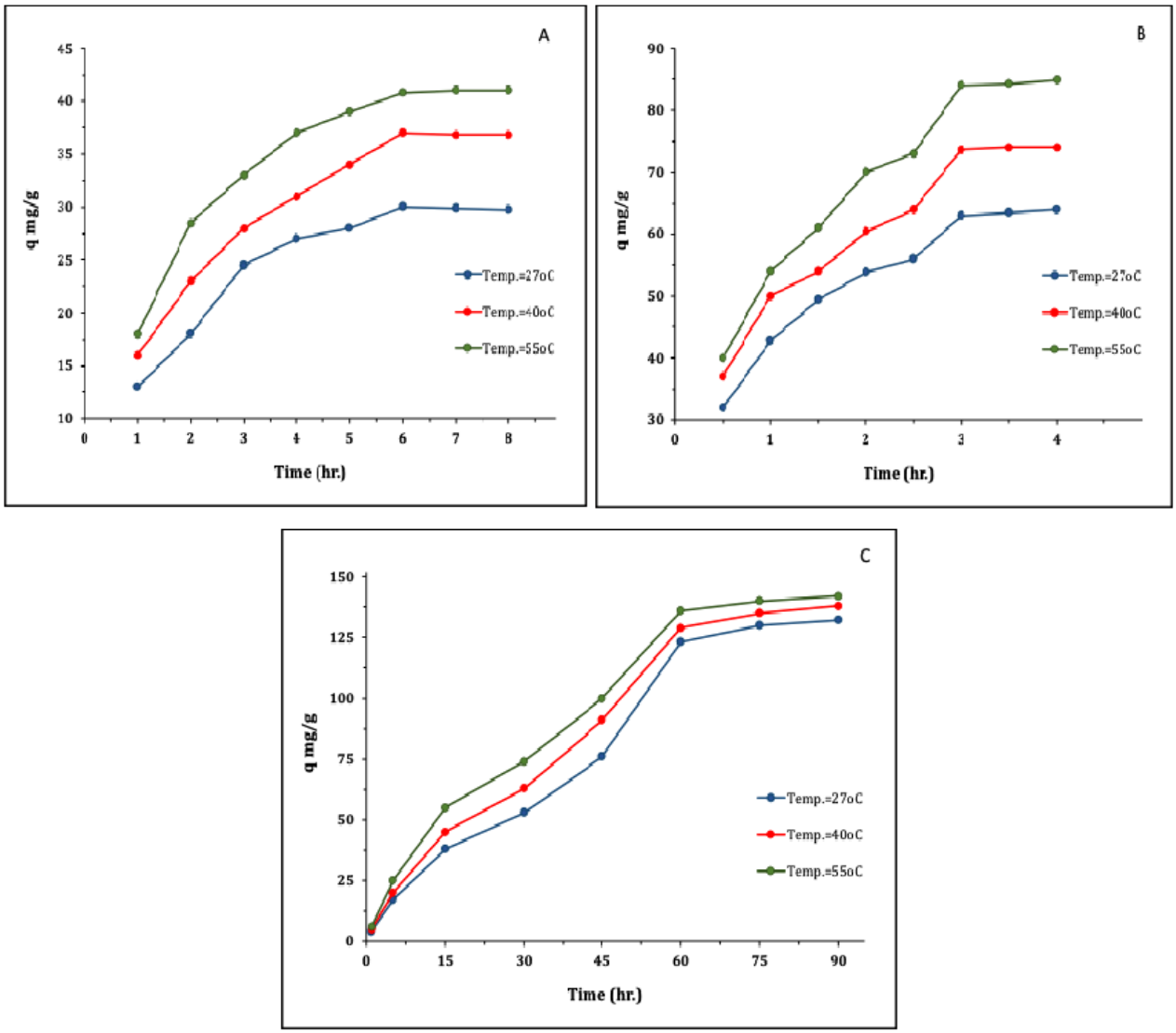


**Fig. 6**. Effect of Agitation time for Cadmium ion onto (A): M@F, (B): M@EDTA@F, (C) M@EDTA@Am@F at 27 °C, 40 °C, and 55 °C.

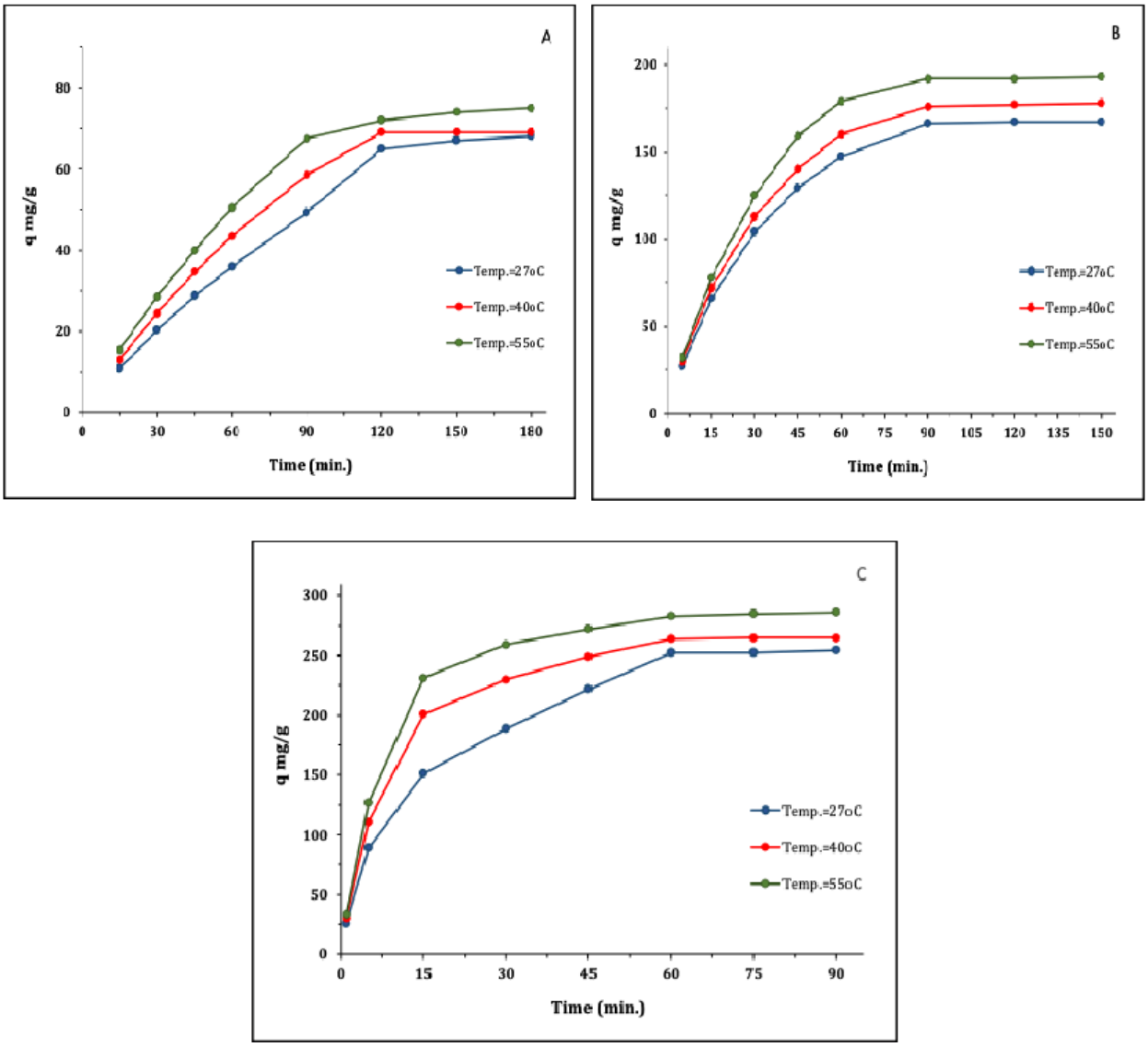


**Fig. 7.** Effect of Agitation time for lead ion onto (A): M@F, (B): M@EDTA@F, (C) M@EDTA@Am@F at 27 °C, 40 °C, and 55 °C.

lead ions respectively had increased rapidly from low agitation time until reach an equilibrium at all temperatures, the results indicated that the equilibrium agitation times for cadmium were 6, 3 and 1 hours and for lead were 2, 1.5 and 1 hours for M@F, M@F, M@EDTA@F, M@EDTA@Am.@F respectively.

### *3.5.3.Adsorption isotherms*

The adsorption isotherms show the equilibrium relationship and interaction between the adsorbent and adsorbate at a specific temperature. Finding the best-fitting isotherms to explain the adsorption process [33]. The adsorption isotherms were examined to establish a basis for determining adsorption capacity, exposing adsorption behavior, and proposing potential adsorption mechanisms [34]. Several isotherm models could be used to describe the experimental data of adsorption models and were applied to the obtained equilibrium data. In this study, Langmuir [35], Freundlich [36], Temkin [37], and Dubinin–Radushkevich [38] models were used. According to the Langmuir model, a monolayer covering of adsorbate molecules forms on a uniform adsorbent surface without any interaction between the molecules.

The most widely used isothermal adsorption model strongly agrees with several experimental data [35]. The Langmuir model's linearized form is provided at Equation 3.

$$\frac{C_e}{q_e} = \frac{1}{q_{max}K_L} + \frac{C_e}{q_{max}}$$

(Eq.3)

Where $q_e$ is the amount adsorbed, $C_e$ is the equilibrium concentration, $q_{max}$ *is* the maximum adsorption capacity reflected on a complete monolayer, and $K_L$ represents the Langmuir constant related to adsorption's apparent energy. The following equation [39] defines the separation factor or equilibrium parameter ($R_L$), which can be used to characterize the key features of the Langmuir isotherms, as shown in Equation 4.

$$R_L = \frac{1}{1+K_L C_e}$$

(Eq.4)

Where $R_L$ values indicate the type of adsorption to be irreversible ($R_L$=0), favorable (0 < $R_L$< 1), linear ($R_L$=1), or unfavorable ($R_L$ > 1), this model is the most commonly used isothermal adsorption model and has demonstrated good agreement with various experimental data [35]. Figures 8A and 8B show the plots of the Langmuir adsorption isotherms of cadmium and lead adsorbed onto M@F, M@EDTA@F, and M@EDTA@Am@F, respectively. Table 1 displays qmax, KL, RL, and the correlation coefficient $R^2$ results for the Langmuir isotherms. The calculated $R_L$ values were found to be equal (0.2301, 0.12939, and 0.61652) for cadmium and (0.57997, 0.55509, and 0.79694) for lead for M@F, M@EDTA@F, and M@EDTA@Am@F, respectively. Under the imposed ideal condition, the computed results demonstrated that all adsorbents were advantageous for adsorbing metal ions from solutions.

The Freundlich adsorption isotherm is an empirical equation widely used for explaining adsorption equilibrium [36]. It is based on adsorption on the surface of a heterogeneous multilayer and assumes that the adsorption takes place at sites with varying energy of adsorption [40]. The Freundlich isotherm is represented as Equation 5.

$$lnq_e = lnK_F + \frac{1}{n} lnC_e$$

(Eq.5)

$K_F$ and n, respectively, are Freundlich constants associated with adsorption intensity and capacity.

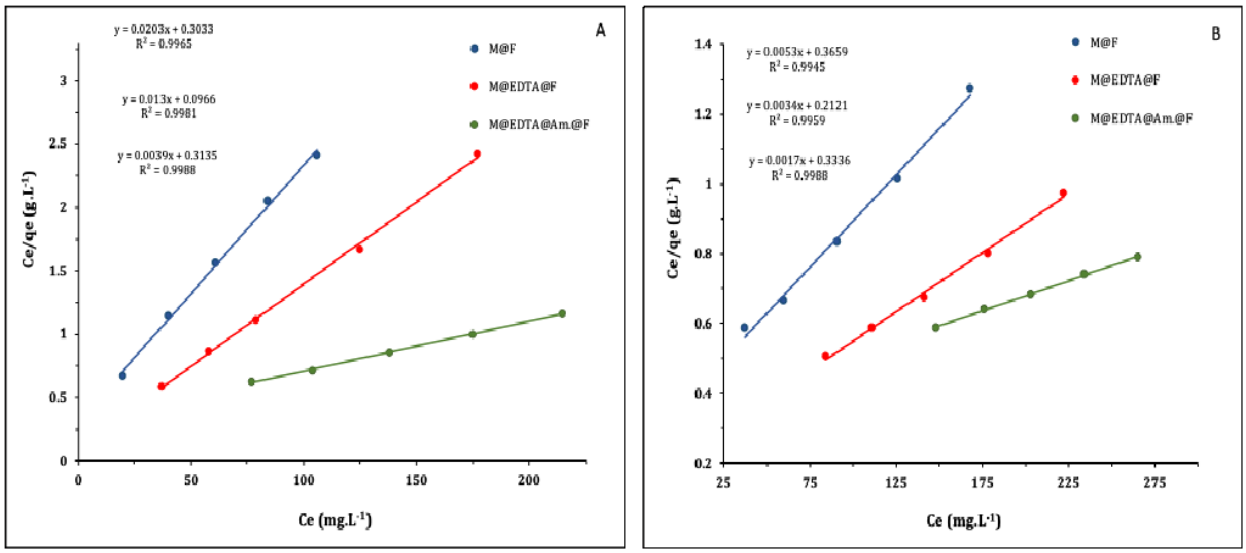


**Fig. 8**. Langmuir isotherm model for (A): Cadmium (B): Lead ion solution at 27 °C

**Table 1**. Langmuir isotherm parameters for adsorption of cadmium and lead ion onto Adsorbents.

| Adsorbent | Cadmium | | | | Lead | | | |
|---|---|---|---|---|---|---|---|---|
| | $q_{max}$ | $K_L$ | $R_L$ | $R^2$ | $q_{max}$ | $K_L$ | $R_L$ | $R^2$ |
| M@F | 49.26 | 0.06693 | 0.2301 | 0.9965 | 188.7 | 0.0145 | 0.57997 | 0.9945 |
| M@EDTA@F | 76.92 | 0.13458 | 0.12939 | 0.9981 | 294.1 | 0.016 | 0.55509 | 0.9959 |
| M@EDTA@Am.@F | 256.4 | 0.0124 | 0.61652 | 0.9988 | 588.2 | 0.0051 | 0.79694 | 0.9988 |

$q_{max}$ (mg $g^{-1}$), k (L $mg^{-1}$)

The n-value measures the degree of surface heterogeneity, which characterizes the distribution of the adsorbed molecules on the adsorbent surface. The KF shows the adsorbent's adsorption capacity toward the adsorbate. Figures 9A and 9B represent the Freundlich adsorption isotherms plots of cadmium and lead ions onto M@F, M@EDTA@F, and M@EDTA@Am@F. Table 2 displays the Freundlich isotherm constants $K_F$, 1/n, and the correlation coefficient $R^2$, which were determined from the plot of *ln* $q_e$ against ln $C_e$; the slope and the intercept are 1/n and $K_F$, respectively. The Freundlich constant, or KF, indicates the adsorbent's ability to adsorb the adsorbate. A higher KF value indicates a greater affinity for the adsorbate [41]. Also, the adsorption capacity of the specified adsorbent rises in tandem with the $K_F$ values [42]. According to the results, $K_F$ indicated that all as-synthesized adsorbents had a higher affinity for lead and cadmium ions. The 1/n is the adsorption intensity, and its magnitude indicates the favorability of adsorption. In general, the value of 1/n gives an idea about the type of isotherm, whether it is irreversible (1/n =0), favorable (0 < 1/n < 1), or unfavorable (1/n > 1) [43]. It can be noticed from Table 2 that all the values of 1/n are less than 1, demonstrating that it is favorable for chemisorption for all adsorption systems of cadmium and lead ions.

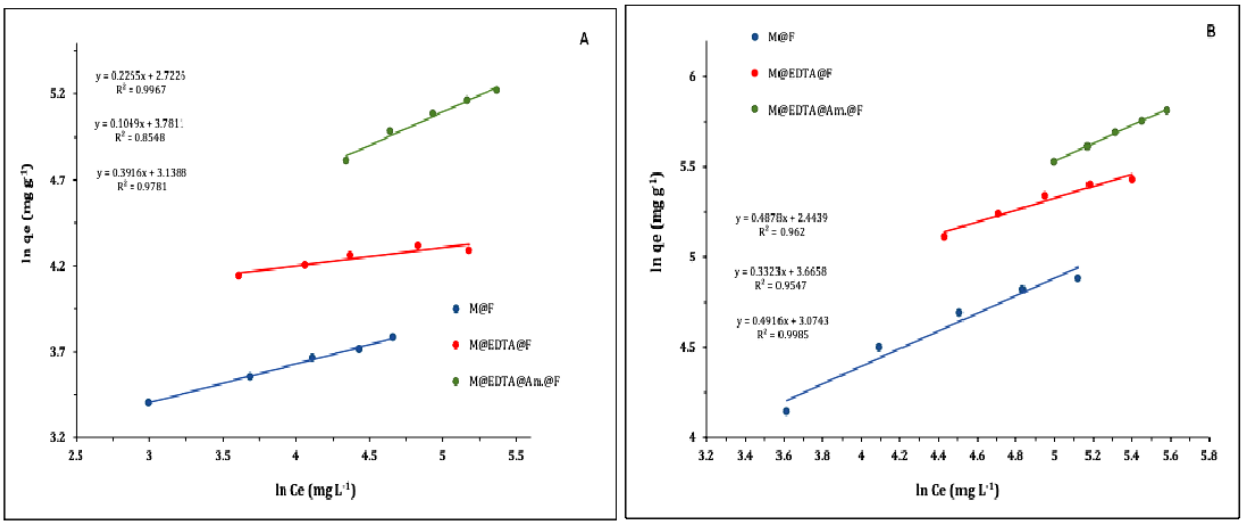


**Fig. 9**. Freundlich isotherm model for (A): Cadmium (B): Lead ion solution at 27°C

**Table 2**. Freundlich isotherm parameters for the adsorption of cadmium and lead ions

| Adsorbent | Cadmium | | | Lead | | |
|---|---|---|---|---|---|---|
| | $K_F$ | 1/n | $R^2$ | $K_F$ | 1/n | $R^2$ |
| M@F | 15.22 | 0.2265 | 0.9967 | 11.518 | 0.4878 | 0.962 |
| M@EDTA@F | 43.864 | 0.1049 | 0.8548 | 39.087 | 0.3323 | 0.9547 |
| M@EDTA@Am.@F | 23.076 | 0.3916 | 0.9781 | 21.635 | 0.4916 | 0.9985 |

$K_F$ (L $mg^{-1}$)

The nature of the adsorption, including its chemical or physical character, is examined via the Dubinin–Radushkevich (D-R) isotherm [44]. Equation 6 shows the linear form of the D-R isotherm model.

$$lnq_e = lnq_{max} + K_D\varepsilon^2$$

(Eq.6)

Where qe and max are the equilibrium adsorption capacity and the maximum adsorption capacity under optimized conditions in the D-R isotherm model, respectively, KD is a constant related to the mean adsorption energy (ED), and ε is the Polanyi potential associated with the equilibrium concentration, as shown in Equation 7. Also, Equation 8 can calculate the mean free energy ED of adsorption per molecule of adsorbate (for removing a molecule from its location in the sorption space to infinity in the solution).

$$\varepsilon = R\,T\,ln\left(1+\frac{1}{C_e}\right)$$

(Eq. 7)

$$E_D = \frac{1}{2K^{1/2}}$$

(Eq. 8)

Figure 10 (A, B) shows plots of the D-R adsorption isotherms of cadmium and lead ions onto M@F, M@EDTA@F, and M@EDTA@Am@F. Table 3 presents the values of D-R isotherm parameters $q_{max}$, $K_D$, $E_D$, and $R^2$, which were determined from the linear plot of $ln\ q_e$ versus $\varepsilon^2$; the slope and intercept of the plot give KD and qmax values, respectively.

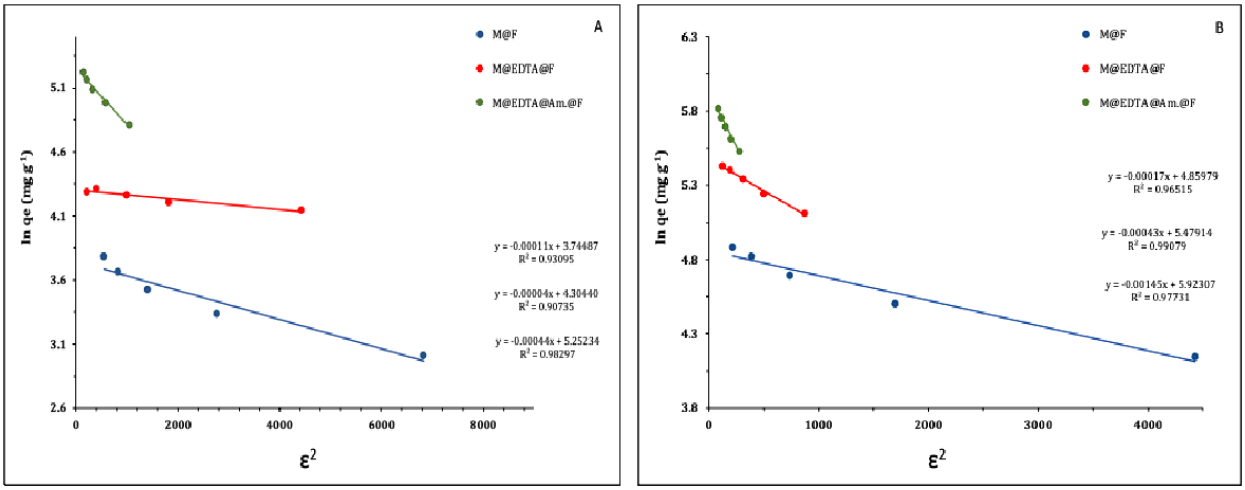


**Fig. 10**. D-R isotherm model for (A): Cadmium (B): Lead ion solution at 27°C

**Table 3**. D-R isotherm parameters for adsorption of cadmium and lead ions onto prepared adsorbents.

| Adsorbent | Cadmium | | | | Lead | | | |
|---|---|---|---|---|---|---|---|---|
| | $q_{max}$ | $K_D$ | $E_D$ | $R^2$ | $q_{max}$ | $K_D$ | $E_D$ | $R^2$ |
| M@F | 42.3048 | 0.00011 | 67.42 | 0.931 | 128.986 | 0.00017 | 54.23 | 0.931 |
| M@EDTA@F | 74.0248 | 3.9E-05 | 113.2 | 0.9073 | 239.641 | 4.3E-05 | 107.8 | 0.9908 |
| M@EDTA@Am.@F | 191.005 | 0.000438 | 33.79 | 0.9829 | 373.568 | 0.001449 | 18.58 | 0.9773 |

$q_{max}$ (mg $g^{-1}$), $K_D$ ($mol^2$ $KJ^{-2}$), $E_D$ (KJ $mol^{-1}$)

Moreover, the D-R model can reveal the adsorption type (physical or chemical adsorption) according to the mean free energy of adsorption ($E_D$). Generally speaking, when the $E_D$ is less than 8.0 kJ mol-1, physical adsorption predominates, whereas when the $E_D$ is greater than 8.0 kJ $mol^{-1}$, chemical adsorption takes the lead [45]. The $E_D$ values exceeded 8.0 kJ $mol^{-1}$, indicating that chemical interactions dominate the adsorption of lead and cadmium ions onto the produced adsorbent.

According to the Temkin isotherm, adsorption is defined by a uniform distribution of binding energies up to a specific maximum binding energy, and the heat of adsorption of all molecules in a layer decreases linearly with coverage as a result of adsorbent-adsorbate interactions [37]. Equation 9 shows the Temkin isotherm in linear form.

$$q_e = B_T ln A_T + B_T ln C_e$$

(Eq. 9)

Where $B_T$, the Temkin constant, is equal to , T (in K) is absolute temperature, R is equal to 8.314 J $mol^{-1}$ $K^{-1}$ is the universal gas constant, $b_T$ (kJ $mol^{-1}$) is related to the heat of adsorption, and $A_T$ (in L $mg^{-1}$) is the equilibrium constant coinciding with maximum binding energy.

Figures 11A and 11B show plots of qe versus lnCe for the Temkin model for the adsorption of cadmium and lead ions onto as-prepared adsorbents. The values of BT and AT are determined from the slope and intercept, which are given in Table 4 along with the correlation coefficient $R^2$ for the Temkin isotherm. Table 1 shows that the Langmuir isotherm model was a better fit than the Freundlich, Dubinin, and Temkin models for removing cadmium and lead by all adsorbents, where the intricacy of adsorption processes was inspired. However, it might be said that there was a propensity for chemical adsorption between metal ions and the functional groups of adsorbents.

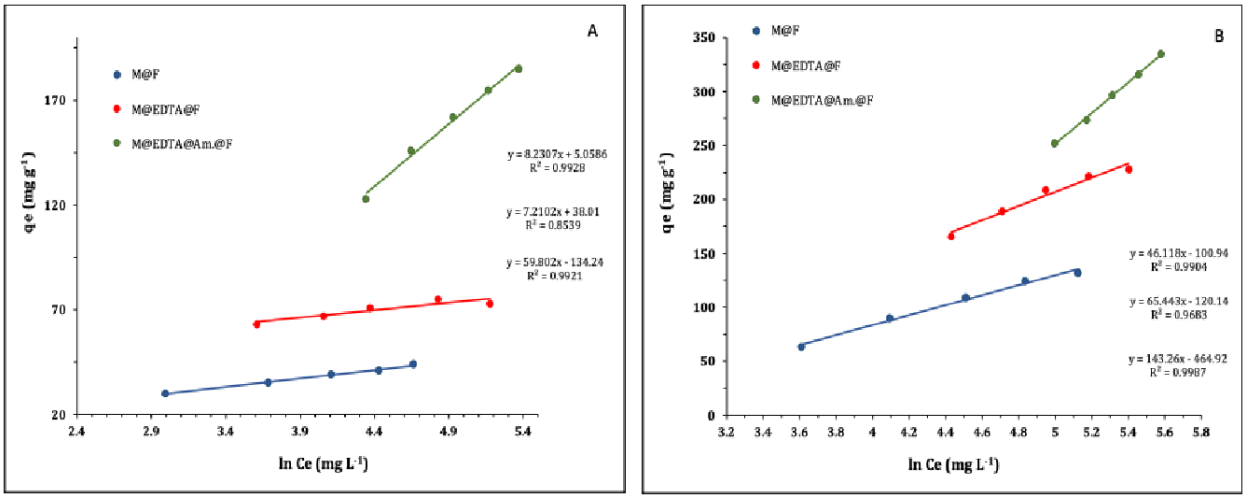


**Fig.11**. Temkin isotherm model for (A): Cadmium (B): Lead ion solution at 27°C

**Table 4**. Temkin isotherm parameters for the adsorption of cadmium and lead ions onto adsorbents

| Adsorbents | Cadmium | | | Lead | | |
|---|---|---|---|---|---|---|
| | $b_T$ | $A_T$ | $R^2$ | $b_T$ | $A_T$ | $R^2$ |
| M@F | 303.0361 | 1.8489 | 0.9928 | 54.083 | 8.9239 | 0.9904 |
| M@EDTA@F | 345.9266 | 194.75 | 0.8539 | 38.1125 | 6.2701 | 0.9683 |
| M@EDTA@Am.@F | 41.7073 | 0.106 | 0.9921 | 17.4103 | 0.0384 | 0.9987 |

$b_T$ (J $mol^{-1}$), $A_T$ (L $mg^{-1}$)

### *3.5.4. Adsorption kinetics*

Two kinetic models were tested to interpret the mechanism of cadmium and lead ions' adsorption onto M@F, M@EDTA@F, and M@EDTA@Am@F. The first model was pseudo-first-order; its mathematical expression is shown by Equation 10.

$$\ln(q_e - q_t) = lnq_1 - k_1 t$$

(Eq. 10)

where $q_t$ and $q_1$ (mg $g^{-1}$) are the amounts of dye adsorbed at time t, and at Equilibrium, respectively, and $k_1$ ($min^{-1}$) is the pseudo-first-order rate constant for adsorption.

Figures 12 and 13 (A, B, C) represent the pseudo-first-order of cadmium and lead ions onto prepared adsorbents by plotting ln(qe-qt) on the Y-axis against t. The slope and intercept of the plot give K1 and q1. Table 5 displays the values of calculated adsorption rate constants k1, maximum adsorption capacity q1, and correlation coefficient $R^2$.

A second kinetic model is pseudo-second-order, expressed in linear form as Equation 11 [46].

$$\frac{t}{q_t} = \frac{1}{k_2 q_2^2} + \frac{t}{q_2}$$

(Eq. 11)

Where $q^2$ is the maximum adsorption capacity for the pseudo-second-order, and $k_2$ is the equilibrium rate constant for pseudo-second-order adsorption.

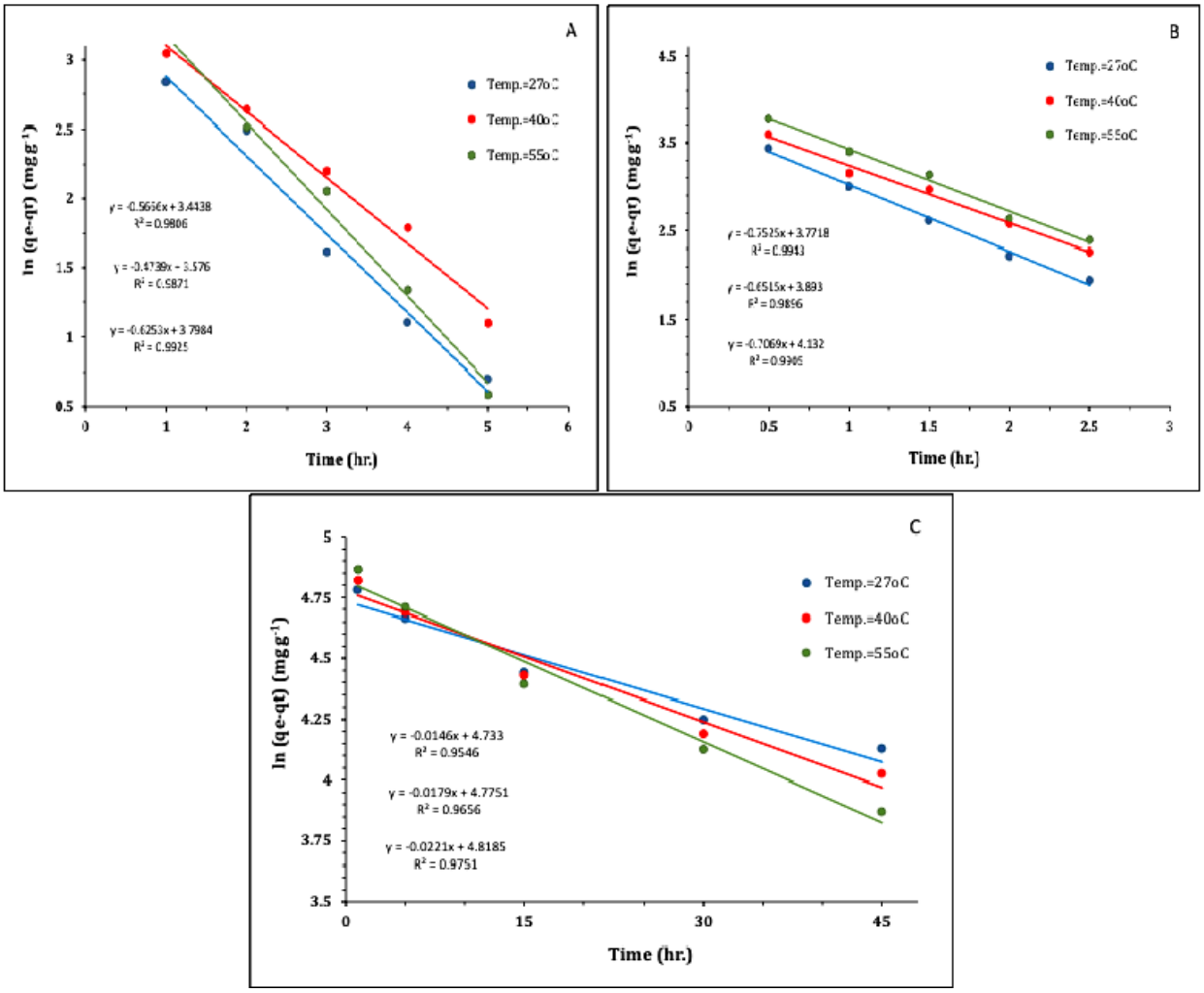


**Fig. 12**. Pseudo-First-Order for Cadmium ion onto (A): M@F (B): M@EDTA@F (C) M@EDTA@Am@F at 27°C, 40°C and 55°C.

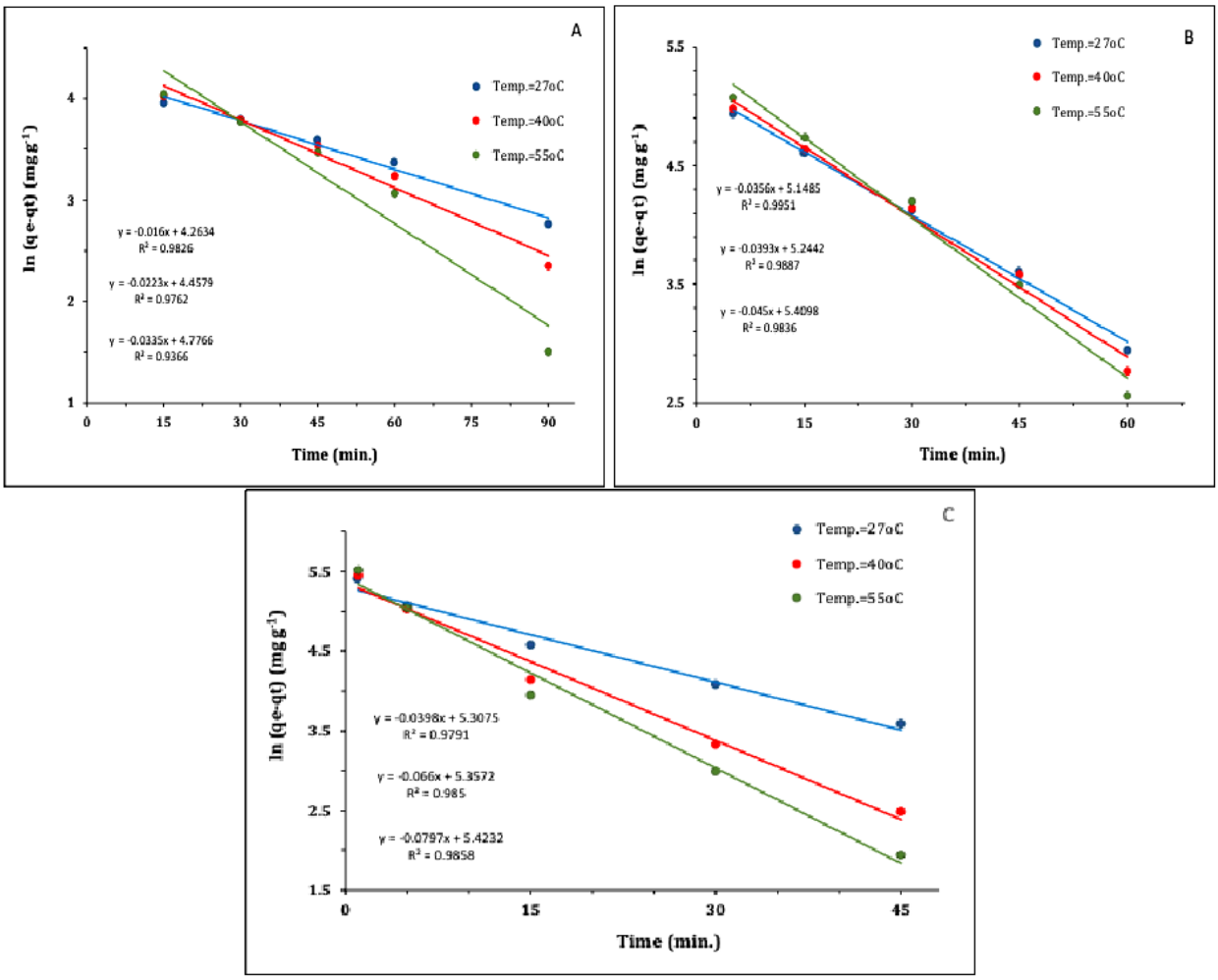


**Fig. 13**. Pseudo-First-Order for Lead ion onto (A): M@F (B): M@EDTA@F (C) M@EDTA@Am@F at 27°C, 40°C and 55°C.

**Table 5**. Pseudo-first-order parameters for adsorption of cadmium and lead ions onto adsorbents at different temperatures.

| Adsorbents | T(°C) | Cadmium | | | Lead | | |
|---|---|---|---|---|---|---|---|
| | | $k_1$ | $q_1$ | $R^2$ | $k_1$ | $q_1$ | $R^2$ |
| M@F | 27 | 0.5666 | 31.3057 | 0.9806 | 0.016 | 71.0511 | 0.9826 |
| | 40 | 0.4739 | 35.7303 | 0.9871 | 0.0223 | 86.3061 | 0.9762 |
| | 55 | 0.6253 | 44.6297 | 0.9925 | 0.0335 | 118.7 | 0.9366 |
| M@EDTA@F | 27 | 0.7525 | 43.4582 | 0.9943 | 0.0356 | 172.173 | 0.9951 |
| | 40 | 0.6515 | 49.0578 | 0.9896 | 0.0393 | 189.464 | 0.9887 |
| | 55 | 0.7069 | 62.3024 | 0.9905 | 0.045 | 223.587 | 0.9836 |
| M@EDTA@ Am.@F | 27 | 0.0146 | 113.636 | 0.9943 | 0.0398 | 201.845 | 0.9791 |
| | 40 | 0.0179 | 118.522 | 0.9896 | 0.066 | 212.13 | 0.9850 |
| | 55 | 0.00221 | 123.779 | 0.9905 | 0.0797 | 226.603 | 0.9858 |

k1 ($min^{-1}$), q ($mg\ g^{-1}$)

Figures 14 and 15 (A, B, C) represent the pseudo-second-order of cadmium and lead ions onto prepared adsorbents, respectively, by plotting t/qt on the Y-axis against t. The slope and intercept of the plot give $k_2$ and $q_2$. Table 6 displays the values of calculated adsorption rate constants $k_2$, maximum adsorption capacity $q_2$, and correlation coefficient $R_2$.

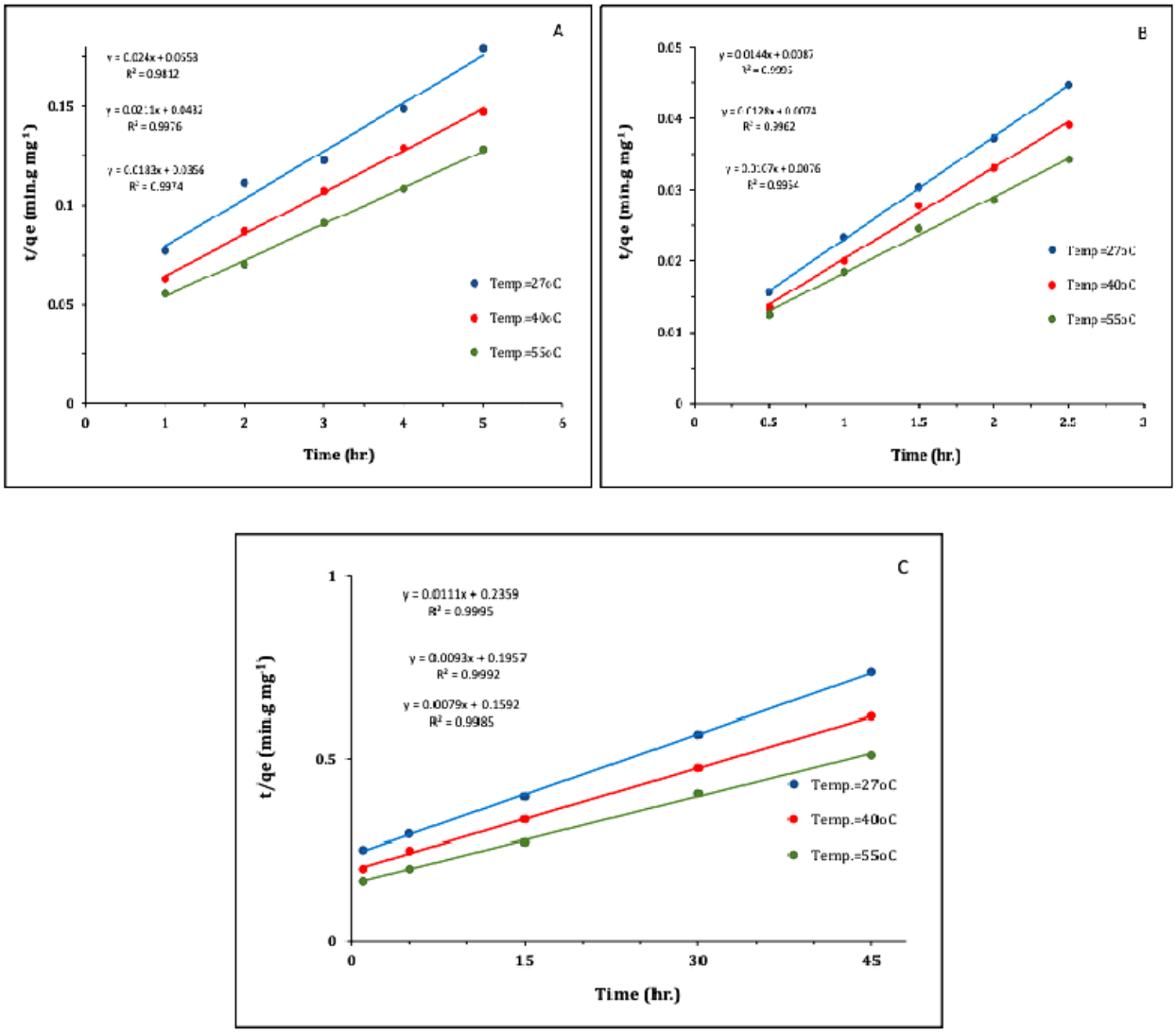


**Fig. 14**. Pseudo-Second-Order for Cadmium ion onto (A): M@F (B): M@EDTA@F (C) M@EDTA@Am@F at 27°C, 40°C and 55°C.

**Table 6**. Pseudo-second-order parameters for adsorption of cadmium and lead ions onto adsorbents at different temperatures.

| Adsorbents | | Cadmium | | | Lead | | |
|---|---|---|---|---|---|---|---|
| | T (°C) | $k_2$ | $q_2$ | $R^2$ | $k_2$ | $q_2$ | $R^2$ |
| M@F | 27 | 0.01042 | 41.6667 | 0.9812 | 2.7E-05 | 169.492 | 0.9987 |
| | 40 | 0.01031 | 47.3934 | 0.9976 | 2.5E-05 | 192.308 | 0.9991 |
| | 55 | 0.00941 | 54.6448 | 0.9974 | 2.4E-05 | 212.766 | 0.9992 |
| M@EDTA@F | 27 | 0.02383 | 69.4444 | 0.9995 | 9.9E-05 | 246.914 | 0.9999 |
| | 40 | 0.02214 | 78.125 | 0.9962 | 9.5E-05 | 264.55 | 0.9994 |
| | 55 | 0.01506 | 93.4579 | 0.9954 | 7.2E-05 | 312.5 | 0.9989 |
| M@EDTA@ Am.@F | 27 | 0.00052 | 90.0901 | 0.9995 | 0.000403 | 256.41 | 0.9987 |
| | 40 | 0.00044 | 107.527 | 0.9992 | 0.000388 | 303.03 | 0.9989 |
| | 55 | 0.00039 | 126.582 | 0.9992 | 0.000377 | 333.333 | 0.9969 |

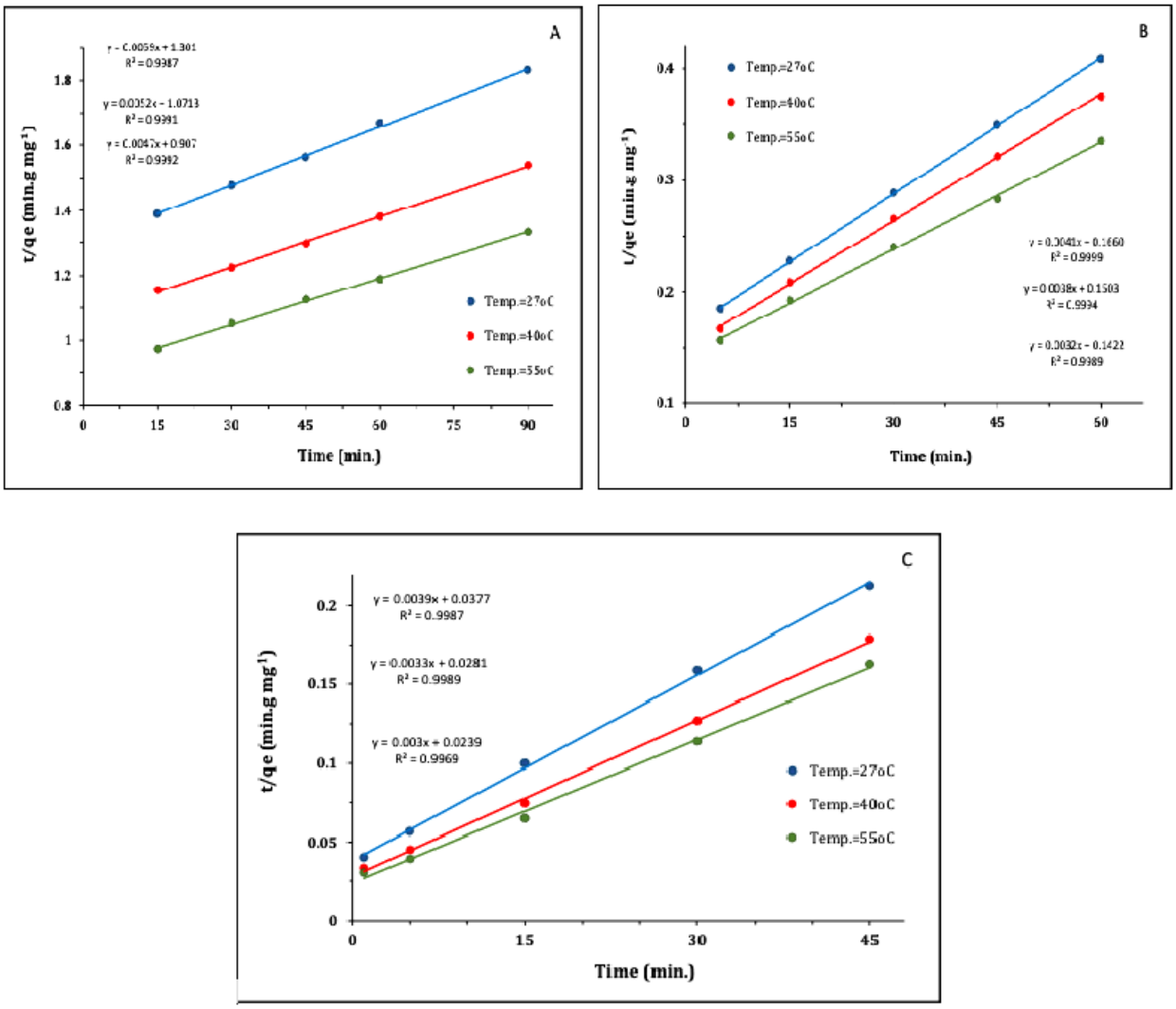


**Fig.15**. Pseudo-Second-Order for Lead ion onto (A): M@F (B): M@EDTA@F (C) M@EDTA@Am@F at 27°C, 40°C and 55°C.

### *3.5.5. Adsorption thermodynamics*

Thermodynamic parameters can be determined from the thermodynamic equilibrium constant, $K_L$ (or the thermodynamic distribution coefficient) [47], whereas $K_L$ is calculated by Equation 12. The standard enthalpy changes $\Delta H°$ (kJ mol$^{-1}$) and standard entropy change) $\Delta S°$ (J mol$^{-1}$ K$^{-1}$) was calculated using Equation 13.

$$K_L = \frac{C_a}{C_e}$$

(Eq. 12)

$$\ln k = \frac{\Delta S^o}{R} - \frac{\Delta H^o}{RT}$$

(Eq. 13)

In Equation 12, $C_a$ and $C_e$ are the equilibrium concentrations of metal ions (mg g$^{-1}$) and in the solution (mg L$^{-1}$). In Equation 13, R is the universal gas constant (8.314 J mol$^{-1}$K$^{-1}$), and T is the absolute temperature. By plotting (ln KL) vs. (1/T), ΔH° can be calculated ΔH° from the slope and ΔS° from the intercept, Figures 16 (A, B). The standard Gibbs free energy ΔG° (in kJ mol$^{-1}$) could be calculated at different temperatures by Equation 14. Activation energy Ea (in kJ mol-1) is defined as the minimum amount of energy

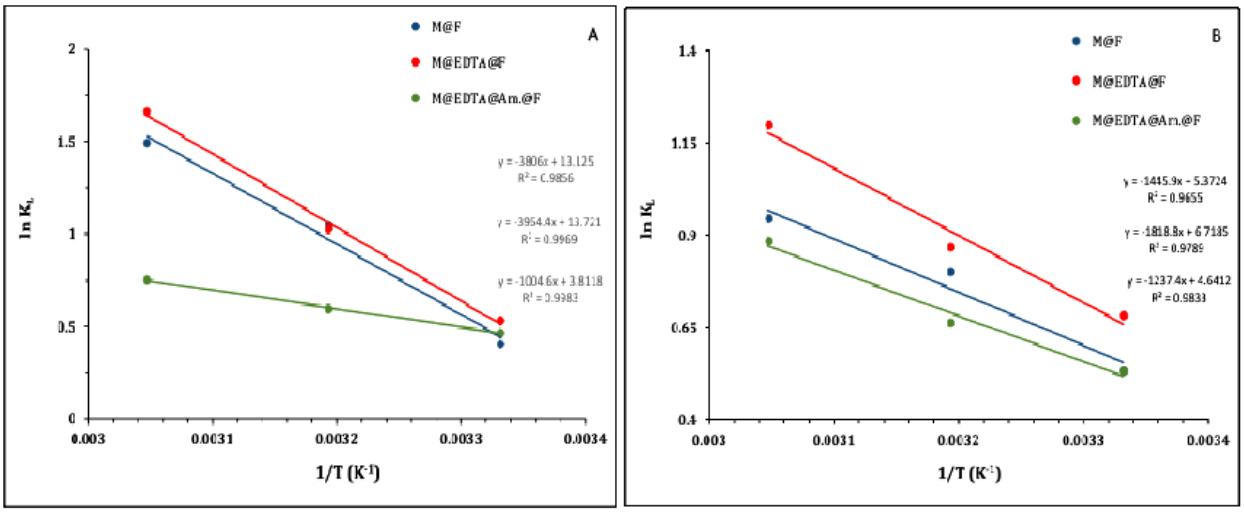


**Fig. 16**. Thermodynamic parameter determination for (A): Cadmium (B): Lead ion solution pH at 27°C

required for the adsorption process to proceed, and it was calculated from the Arrhenius Equation 15.

$$\Delta G^o = \Delta H^o - T\Delta S^o$$

(Eq. 14)

$$ln\ K = ln\ A - \frac{E_a}{RT}$$

(Eq. 15)

Where K ( g $mg^{-1}$ $min^{-1}$) is the rate constant of the pseudo-second order adsorption systems, A is the Arrhenius factor, when (lnK) is plotted against (1/T), a slope equal to -Ea/R as shown in Figure 17A and Figure 17 B. The values of ΔH°, ΔS°, ΔG°, and Ea for the adsorption of metal ions onto adsorbents M@F, M@EDTA@F, and M@EDTA@Am@F are shown in Table 7.

The calculated thermodynamic parameters show positive enthalpy (ΔH°) values for all adsorbents, indicating endothermic adsorption processes. Also, the positive value of entropy (Δ*S*°) suggests an increase in the randomness at the (adsorbents/

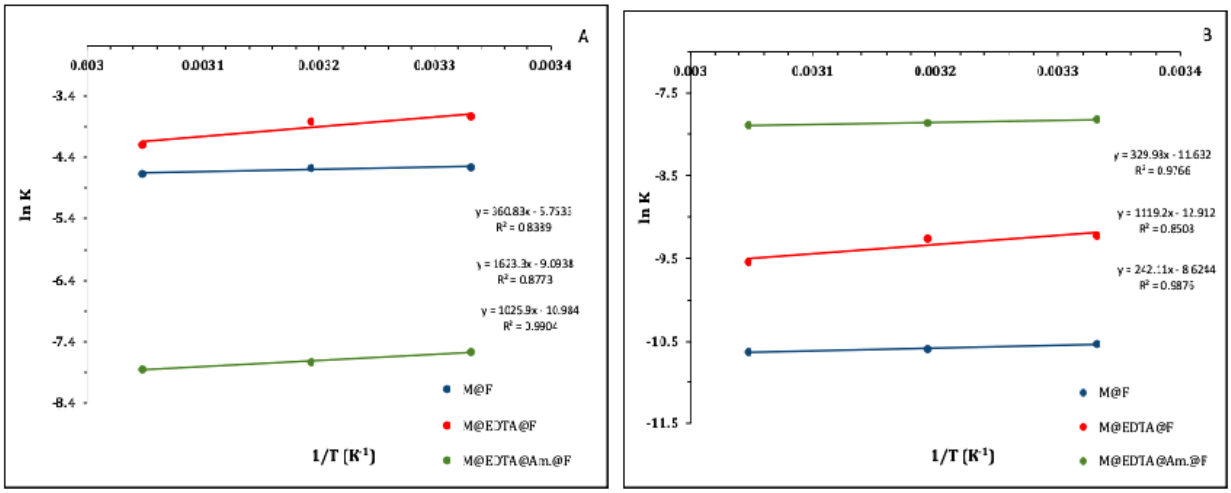


**Fig. 17**. Plot of *lnK* vs. *1/K* of Arrhenius equation for (A): Cadmium (B): Lead ion solution pH at 27°C.

**Table 7**. Thermodynamic parameters for the adsorption of cadmium and lead ions onto prepared adsorbents at different temperatures

| Adsorbents | | Cadmium | | | | Lead | | | |
|---|---|---|---|---|---|---|---|---|---|
| | T(°K) | ΔH° | **ΔS°** | **-ΔG°** | **Ea** | **ΔH°** | **ΔS°** | **-ΔG°** | **Ea** |
| M@F | 300.15 | 31.64 | 0.1091 | -1.109 | -2.999 | 12.0212 | 0.04467 | -1.38608 | -2.743 |
| | 313.15 | | | -2.528 | | | | -1.96677 | |
| | 328.15 | | | -4.165 | | | | -2.6368 | |
| M@EDTA@F | 300.15 | 32.96 | 0.1141 | -1.2800 | -13.49 | 15.1215 | 0.05586 | -1.64416 | -9.305 |
| | 313.15 | | | -2.763 | | | | -2.37031 | |
| | 328.15 | | | -4.47415 | | | | -3.20817 | |
| M@EDTA@Am.@F | 300.15 | 8.35 | 0.0317 | -1.1599 | -8.529 | 10.2877 | 4.6412 | -1.29413 | -2.0129 |
| | 313.15 | | | -1.57189 | | | | -1.79576 | |
| | 328.15 | | | -2.04726 | | | | -2.37456 | |

solution) interface and affinity of the mentioned adsorbents towards metal ions. [48]. The obtained values of Gibbs free energy changes, ΔG°, at different temperatures were negative for all adsorption systems, indicating that the behavior of adsorption processes is spontaneous and feasible [49]. Low activation energy Ea values (<40 kJ $mol^{-1}$) are characteristics of the physisorption mechanism. Whereas higher activation energies more than 40 KJ $mol^{-1}$ suggest chemisorption [50]. Therefore, these results indicate that the adsorption processes of metal ions onto M@F, M@EDTA@F, and M@EDTA@Am@F were physical.

## 4. Conclusion

This work examined three magnetic nanocomposites, M@F, M@EDTA@F, and M@EDTA@Am@F, to evaluate their applicability for removing $Cd^{2+}$ and $Pb^{2+}$. The maximum adsorption of metal ions onto the prepared adsorbents was obtained at 27°C and pH 8.0 for cadmium and 5.0 for lead. Adsorption capacity for metal ions increased with an increase in the initial concentration. The concentrations of Heavy Metal Ions were determined with flame atomic absorption spectroscopy. The kinetic modeling of $Cd^{2+}$ and $Pb^{2+}$ adsorption onto the prepared adsorbents well followed the pseudo-second-order rate model, with the correlation coefficients of higher than 0.99. A monolayer Langmuir-type isotherm for M@F, M@EDTA@F, and M@EDTA@Am@F describes adsorption behavior. The calculated thermodynamic parameters show positive enthalpy (ΔH°) values for all adsorbents, indicating endothermic adsorption processes. Also, the positive value of entropy (Δ*S*°) suggests an increase in the randomness at the (adsorbents/solution) interface and affinity of the mentioned adsorbents towards metal ions. The negative values of ΔG° at different temperatures indicate that the behavior of adsorption processes is spontaneous and feasible. Low activation energy Ea values are characteristics of the physisorption mechanism and diffusion-controlled process.

## 5. Acknowledgements

We thank and appreciate the University of Basrah, College of Science, Chemistry Department - Basrah, Iraq

## 6. References

[1] C. Rupa, A. Anupama, S. Ajaya Kumar, J. Bhawana, H. Susan, A review of adsorption of heavy metal ions by various low-cost adsorbents, Int. J. Environ. Anal. Chem., 102 (2020) 342-379. https://doi.org/10.1080/03067319.2020.1722811

[2] M. Arjomandi, A review: analytical methods for heavy metals determination in environment and human samples, Anal. Methods Environ. Chem. J., 2 (2019) 97-126. https://doi.org/10.24200/amecj.v2.i03.73

[3] V. Srivastava, C.H. Weng, V.K. Singh, Y.C.

Sharma, Adsorption of nickel ions from aqueous solutions by nano alumina: kinetic, mass transfer, and equilibrium studies, J. Chem. Eng. Data, 56 (2011) 1414-1422. https://doi.org/10.1021/je101152b

[4] H. Zhang, M. Reynolds, Cadmium exposure in living organisms: A short review, Sci. Total Environ., 678 (2019) 761–767. https://doi.org/10.1016/j.scitotenv.2019.04.395

[5] S. Malar, S. Shivendra, P. Favas, V. Perumal, Lead heavy metal toxicity induced changes in growth and the level of antioxidative enzymes in water hyacinths, Bot. Stud., 55 (2014) 54. https://doi.org/10.1186/s40529-014-0054-6

[6] J. Mirosławski, A. Paukszto, Determination of the Cd, chromium, nickel, and lead ions relays in selected polish medicinal plants and their infusion, Biol. Trace Elem. Res., 182 (2017) 147–151. https://doi.org/10.1007/s12011-017-1072-5

[7] J. Kasten-Jolly, D.A. Lawrence, Sex-specifc efects of developmental lead exposure on the immune-neuroendocrine network, Toxicol. Appl. Pharmacol., 334 (2017) 142–157. https://doi.org/10.1016/j.taap.2017.09.009

[8] A. Kumar, A. Kumar, M. Cabral-Pinto, A.K. Chaturvedi, A. Shabnam, G. Subrahmanyam, R. Mondal, Lead toxicity health hazards, influence on food chain, and sustainable remediation approaches, Int. J. Environ. Res. Public Health, 17 (2020) 2179. https://doi.org/10.3390/ijerph17072179

[9] S. Kumar, R. Islam, P. Bhowmik, G.R. Macfarlane, Lead (Pb) contamination in agricultural products and human health risk assessment in Bangladesh, Water Air Soil Pollut., 233 (2022) 257. https://doi.org/10.1007/s11270-022-05711-9

[10] A. Rashidi, A. Vahid, Arsenic speciation based on amine-functionalized bimodal mesoporous silica nanoparticles by ultrasound assisted-dispersive solid-liquid multiple phase microextraction, Microchem. J., 130 (2017) 137-146. https://doi.org/10.1016/j.microc.2016.08.013

[11] J. Rakhtshah, M. Dehghani Mobarake, Simultaneously speciation and determination of manganese (II) and (VII) ions in water, food, and vegetable samples based on immobilization of N-acetylcysteine on multi-walled carbon nanotubes, Food Chem., 389 (2022) 133124. https://doi.org/10.1016/j.food chem.2022.133124

[12] A. F. Zarandi, An immobilization of 2-(Aminomethyl) thiazole on MWCNTs used for rapid extraction of manganese ions in hepatic patients, J. Pharm. Biomed. Anal., 240 (2024) 115941. https://doi.org/10.1016/j.jpba.2023.115941

[13] Z. Karamzadeh, A novel biostructure sorbent based on CysSB/MetSB@ MWCNTs for separation of nickel and cobalt in biological samples by ultrasound assisted-dispersive ionic liquid- suspension solid phase microextraction, J. Pharm. Biomed. Anal., 172 (2019) 285-294. https://doi.org/10.1016/j.jpba.2019.05.003

[14] M. M. Eskandari, Cloud point assisted dispersive ionic liquid-liquid microextraction for chromium speciation in human blood samples based on isopropyl 2-[(isopropoxycarbothiolyl)disulfanyl] ethane thioate, Anal. Chem. Res., 10 (2016) 18-27. https://doi.org/10.1016/j.ancr.2016.10.002

[15] M. M. Eskandari, B. Kalantari, Dispersive liquid-liquid microextraction based on task-specific ionic liquids for determination and speciation of chromium in human blood, J. Anal. Chem., 70 (2015) 1448-1455. https://doi.org/10.1134/S1061934815120072

[16] M. K. Abbasabadi, F. Hosseini, Nanographene oxide modified phenyl methanethiol nanomagnetic composite for rapid separation of aluminum in wastewaters, foods, and vegetable samples by microwave dispersive, Food Chem., 347 (2021) 129042. https://doi.org/10.1016/j.foodchem.2021.129042

[17] M. K. Abbasabadi, Speciation of cadmium in human blood samples based on $Fe_3O_4$-

supported naphthalene-1-thiol- functionalized graphene oxide nanocomposite by ultrasound-assisted dispersive magnetic micro solid phase extraction, J. Pharm. Biomed. Anal., 189 (2020)113455. https://doi.org/10.1016/j.jpba.2020.113455

[18] N. Esmaeili, J. Rakhtshah, Ultrasound assisted-dispersive-modification solid-phase extraction using task-specific ionic liquid immobilized on multiwall carbon nanotubes for speciation and determination mercury in water samples, Microchem. J., 154 (2020) 104632. https://doi.org/10.1016/j.microc.2020.104632

[19] N. Esmaeili, J. Rakhtshah, Rapid speciation of lead in human blood and urine samples based on MWCNTs@DMP by dispersive ionic liquid-suspension-micro-solid phase extraction, Biol. Trace Elem. Res., 199 (2021) 2496–2507. https://doi.org/10.1007/s12011-020-02382-7

[20] M. Alaa, Preparation of graphene oxide-grafted polymers and the analytical study of their interaction with Congo Red and Bismarck brown dyes, Thesis for PhD, University of Basra, Iraq, 2020. https://en.sci.uobasrah.edu.iq/1phddepartment-theses-and-dissertation

[21] Q. Nada. Synthesis and characterization of some new 1,3-thiazines and their complexes and evaluation of their adsorption capacity for water remediation, University of Basra, Iraq, 2019. https://en.ceq.uobasrah.edu.iq/

[22] S. Huda. Removal of Carcinogenic Dyes Congo red (CR) and Bismarck brown Y (BBY) by Adsorption onto Reusable Hydrogels Derived from Acrylamide, J. Phys. Conf. Ser., 2063 (2021) 012011. https://doi.org/10.1088/1742-6596/2063/1/012011

[23] H. Fereshte, D. Haniyeh, E. Farhad, M. Ali, Magnetized melamine-modified polyacrylonitrile (PAN@melamine/$Fe_3O_4$) organometallic nanomaterial: Preparation, characterization, and application as a multifunctional catalyst in the synthesis of bioactive dihydropyrano [2,3-c]pyrazole and 2-amino-3-cyano4H-pyran derivatives, Appl. Organometal. Chem., 35 (2021) e6363. https://doi.org/10.1002/aoc.6363

[24] G. Weixing, Y. Haibing, Z. Yifu, Q. Sheldon, L. Cuiwu, P. Licheng, H. Zhoufeng, Synthesis and characterization of sucrose-melamine-formaldehyde adhesives, BioResour., 11 (2016) 2516-2525. https://doi.org/10.15376/biores.11.1.2516-2525

[25] S. Jumat, S. Nadia, Y. Emad, Synthesis and characterization of esters derived from ricinoleic acid and evaluation of their low-temperature property, Sains Malays., 41 (2012) 1239–1244. https://www.researchgate.net/publication/279640936

[26] L. Zhang, H. Luo, P. Liu, W. Fang, J. Geng, A novel modified graphene oxide/chitosan composite used as an adsorbent for Cr (VI) in aqueous solutions, Int. J. Biol. Macromol., 87 (2016) 586-596. https://doi.org/10.1016/j.ijbiomac.2016.03.027

[27] A. Monshi, M. Foroughi, M.R. Monshi, Modified Scherrer equation to estimate more accurately nano-crystallite size using XRD, World J. Nano Sci. Eng., 2 (2012) 154–160. https://doi.org/10.4236/wjnse.2012.23020

[28] R. Yong, A. Hayder, H. Fengbo, P. Hong, H. Kaixun, Magnetic EDTA-modified chitosan/$SiO_2$/$Fe_3O_4$ adsorbent: Preparation, characterization, and application in heavy metal adsorption, Chem. Eng. J., 226 (2013) 300–311. https://doi.org/10.1016/j.cej.2013.04.059

[29] M. Ahamed, H. Alhadlaq, M. Khan, P. Karuppiah, N. Al-Dhabi, Synthesis, characterization, and antimicrobial activity of copper oxide nanoparticles, J. Nanomater., 2014 (2014) 37858. https://doi.org/10.1155/2014/637858

[30] A. Y. Hammo, T. E. Jassim, M. J.K. AL. Asadi, Preparation and characterization of some ferrite spinal magnetic nanocomposites and their use as adsorbent surfaces to treat elemental and oil pollution from their

aqueous solutions, India. J. Ecol., 49 (2022) 675-683. https://faculty.uobasrah.edu.iq/uploads/publications/1650953836.pdf

[31] S. D. Ahranjani, A lead analysis based on amine-functionalized bimodal mesoporous silica nanoparticles in human biological samples by ultrasound assisted-ionic liquid trap-micro solid phase extraction, J. Pharm. Biomed. Anal., 157 (2018) 1-9. https://doi.org/10.1016/j.jpba.2018.05.004

[32] S. Mishra, D. Mohapatra, D. Mishra, P. Chattopadhyay, G. Chaudhury, R. Das, Arsenic adsorption on natural minerals, J. Mater. Environ. Sci., 5 (2014) 350-359. https://www.jmaterenvironsci.com/Document/vol5/vol5_N2/41-JMES-455-2013-Mishra.pdf

[33] C. Shih, J. Park, D. Sholl, M. Realff, T. Yajima, Y. Kawajiri, Hierarchical Bayesian estimation for adsorption isotherm parameter determination, Chem. Eng. Sci., 214 (2020) 115435. https://doi.org/10.1016/j.ces.2019.115435

[34] Y. Kuang, X. Zhang, S. Zhou, Adsorption of methylene blue in water onto activated carbon by surfactant modification, Water, 12 (2020) 587. https://doi.org/10.3390/w12020587

[35] A. Sulaymon, T. Mohammed, J. Al-Najar, Equilibrium and kinetics studies of adsorption of heavy metals onto activated carbon, Can. J. Chem. Eng. Tech., 3 (2012) 86–92. https://www.researchgate.net/publication/281526794

[36] A. A. Ansari, S.S. Gill, R. Gill, G. Lanza, L. Newman, Phytoremediation. Springer. 2016. https://doi.org/10.1007/978-3-319-41811-7

[37] Y. Meshram, J. Gunjate, R. Khope, Studies on adsorption characteristics of manganese onto coal based chemically modified activated carbon, Mater. Today Proc., 29 (2020) 1185-1191. https://doi.org/10.1016/j.matpr.2020.05.428

[38] S. Rengaraj, J. Yeon, Y. Kim, Y. Jung, Y. Ha, W. Kim, Adsorption characteristics of Cu(II) onto ion exchange resins 252H and 1500H: Kinetics, isotherms and error analysis, J. Hazard. Mater., 143 (2007) 469–477. https://doi.org/10.1016/j.jhazmat.2006.09.064

[39] R. Gautam, A. Mudhoo, G. Lofrano, M. Chattopadhyaya, Biomass-derived biosorbents for metal ions sequestration: Adsorbent modification and activation methods and adsorbent regeneration, J. Enviro. Chem. Eng., 2 (2014) 239–259. https://doi.org/10.1016/j.jece.2013.12.019

[40] A. F. Zarandi, P. Paydar, A novel method based on functionalized bimodal mesoporous silica nanoparticles for efficient removal of lead aerosols pollution from air by solid-liquid gas-phase extraction, J. Environ. Health Sci. Eng., 18 (2020) 177–188. https://doi.org/10.1007/s40201-020-00450-7

[41] P. Luo, B. Zhang, Y. Zhao, J. Wang, H. Zhang, J. Liu, Removal of methylene blue from aqueous solutions by adsorption onto chemically activated halloysite nanotubes, Korean J. Chem. Eng., 28 (2011) 800–807. https://doi.org/10.1007/s11814-010-0426-x

[42] R. García, R. Medina, M. Lozano, I. Pérez, M. Valero, A. Maubert, Adsorption of azo-dye Orange II from aqueous solutions using a metal-organic framework material: Iron- benzenetricarboxylate, Materials, 7 (2014) 8037–8057. https://doi.org/10.3390/ma7128037

[43] A. S. Muhammad, Adsorption of Methylene blue onto modified agricultural waste, Mor. J. Chem., 8 (2020) 412-427. https://doi.org/10.48317/IMIST.PRSM/morjchem-v8i2.16692

[44] F. Togue Kamga, Modeling adsorption mechanism of paraquat onto Ayous (Triplochiton scleroxylon) wood sawdust, Appl. Water Sci., 9 (2019) 1. https://doi.org/10.1007/s13201-018-0879-3

[45] H. Joga, P. King, Y. Prasanna, Application of response surface methodology for optimization of cadmium adsorption in an aqueous solution by activated carbon prepared from Bauhinia Purpurea leaves,

Rasayan J. Chem., 11 (2018) 1577–1586. https://doi.org/10.31788/RJC.2018.1144024

[46] Y. Ho, G. McKay, Pseudo-second order model for sorption processes, Process Biochem., 34 (1999) 451–465. https://doi.org/10.1016/S0032-9592(98)00112-5

[47] M. D. Mobarake, Ultrasound-assisted solid-liquid trap phase extraction based on functionalized multi-wall carbon nNanotubes for preconcentration and separation of nickel in petrochemical waste water, J. Anal. Chem., 74 (2019) 865-876. https://doi.org/10.1134/S1061934819090090

[48] Y. Önal, C. Akmil-Başar, D. Eren, C. Sarıcı-Özdemir, T. Depci, Adsorption kinetics of malachite green onto activated carbon prepared from Tunçbilek lignite, J. Hazard. Mater., 128 (2006) 150-157. https://doi.org/10.1016/j.jhazmat.2005.07.055

[49] D. Lin, F. Wu, Y. Hu,T. Zhang, C. Liu, Q. Hu, Y. Hu, Z. Xue, H. Han, T. Ko, Adsorption of dye by waste black tea powder: parameters, kinetic, equilibrium, and thermodynamic studies, J. Chem., 2020 (2020) 431046. https://doi.org/10.1155/2020/5431046

[50] A. Swelam, M. Awad, Y. Gedamy, A. Tawfik, $Fe_3O_4$ nanoparticles: Synthesis, characterization and application in removal of iron from aqueous solution and groundwater, Egypt. J. Chem., 62 (2019) 709-789. https://doi.org/10.21608/ejchem.2019.5527.1488